Title
Cooperation, Competition and Specialized Metabolism in a Simplified Root Nodule Microbiome

Author
Hansen, Bridget Lynn

Publication Date
2021

Peer reviewed|Thesis/dissertation

Cooperation, Competition and Specialized Metabolism in a Simplified Root Nodule Microbiome

By

Bridget Lynn Hansen

A dissertation submitted in partial satisfaction of the

requirements for the degree of

Doctor of Philosophy

in

Microbiology

in the

Graduate Division

of the

University of California, Berkeley

Committee in charge:

Professor Matthew F. Traxler, Chair
Professor Michi Taga
Professor Ellen Simms

Spring 2021

Abstract

Cooperation, Competition and Specialized Metabolism in a Simplified Root Nodule Microbiome

by

Bridget Lynn Hansen

Doctor of Philosophy in Microbiology

University of California, Berkeley

Professor Matthew F. Traxler, Chair

Microbes occupy diverse habitats, forming interconnected, dynamic communities. Microbiomes associated with various plant structures often contain members with the potential to make specialized metabolites, e.g. molecules with antibacterial, antifungal, or siderophore activities. However, when and where microbes associated with plants produce specialized metabolites, and the potential role of these molecules in mediating intra-microbiome interactions, is not well understood. Root nodules of legume plants are organs devoted to hosting symbiotic bacteria that fix atmospheric nitrogen and have recently been shown to harbor a relatively simple accessory microbiome containing members with the ability to produce specialized metabolites *in vitro*. Based on these observations, we sought to develop a model nodule microbiome system for evaluating microbial specialized metabolism *in planta*. Starting with an inoculum derived from field-grown *Medicago sativa* nodules, serial passaging through gnotobiotic nodules yielded a simplified accessory community composed of four members: *Brevibacillus brevis, Paenibacillus sp., Pantoea agglomerans,* and *Pseudomonas sp.*. Some members of this community exhibited clear cooperation *in planta*, while others were antagonistic and capable of disrupting cooperation between other partners. Using matrix-assisted laser desorption/ionization imaging mass spectrometry, we found that metabolites associated with individual taxa had unique distributions, indicating that some members of the nodule community were spatially segregated, accounting for their ability to co-exist. Finally, we identified two families of molecules produced by *B. brevis in planta* as the antibacterial tyrocidines and a novel set of gramicidin-type molecules, which we term the britacidins. Collectively, these results indicate that in addition to nitrogen fixation, legume root nodules are likely also sites of active antimicrobial production.

Table of Contents

Acknowledgements

I would like to acknowledge all of those who have contributed to the work described in this dissertation directly or indirectly, and those who have provided insightful discussion, mentorship and direction throughout my matriculation.

I would like to start by expressing my deepest gratitude for my advisor, Dr. Matthew F. Traxler. He has served as an incredible mentor, providing me the freedom to think creatively and speak freely, fostering a productive and exciting environment for discovery and has always believed in me. He has helped me grow as a scientist and as a person, and for that, I am grateful. There have been more than a few times I have gone off into the woods with my investigations and he has never shamed me for it. If anything, he has supported my curiosity and my need for exploration. Thank you, Matt, I cannot fully put into words how incredible this experience has been and how grateful I am for the opportunity to work with you.

I would like to acknowledge my thesis committee members, Dr. Michi Taga and Dr. Ellen Simms. These women have served as scientific mentors and role models. Both Dr. Taga and Dr. Simms have modelled what it means to be strong female scientists and mentors. Their endless support and words of wisdom have helped mold me into the scientist that I am. I am eternally grateful.

I would like to acknowledge my dear friend and most influential mentor, Dr. Rita de Cassia Pessotti. Her and I began the Traxler lab around the same time with similar project goals. We started as colleagues and have become very good friends. She has taught me so much about the microbial chemical world and without her direct help, this work would not have been possible. She was my sounding board, my confidant and my collaborator. She is an incredible tour de force and I can only hope to be as strong a scientist one day.

I would like to thank Dr. Monika Fischer and Mira Liu for their contributions on this project and their constant support as colleagues and friends. I would also like to thank two outstanding undergraduates I had the great fortune to mentor, Laila El-Hifnawi and Alyssa Collins. Without these two, this work would have been physically impossible. They processed hundreds of plants alongside me and will always be known as the dream team.

I would also like to thank my cohort and the Traxler lab as a whole, without their insightful feedback and their constant support, this work would not have been as enjoyable. Dr. Bailey Bonet and Dylan McClung consistently provided feedback during group meetings that ultimately made me a better scientist. They were also the two who helped me the most through qualifying exams.

I would like to acknowledge several facilities. This work was carried out in Koshland Hall and without working autoclaves and double distilled water, this work would have never happened. The Barker hall and QB3 sequencing facilities, the microscopy facility and the NMR facility were instrumental to this work. In addition, without the support of the Oxford Tract, Hopland Field station and Alturas Ranches we would have been unable to carry out this work.

Dedications

For my parents, Robert and Delinda Hansen, and my brother, Robert Hansen III. I love you guys.

Chapter 1: Introduction

A portion of this chapter has been adapted from the following with permission:
Pessotti, R.C., Hansen, B.L., and Traxler, M.F. (2018) In search of model ecological systems for understanding specialized metabolism. mSystems. 3:e00175-17. https://doi.org/10.1128/mSystems.00175-17.

1.1 Microbiomes and specialized metabolism

Microbes occupy diverse habitats and seldom live alone. Microbes have spent roughly the past four billion years evolving in the context of interactive communities, surrounded by thousands of other microorganisms. Environments like soil(1), plants(2) and animals(3) are teaming with microbes. With hundreds to thousands of species present, this level of complexity can be difficult to study. In the past decade, affordable next-generation sequencing has enabled deep profiling of the microbial biodiversity found in a wide array of ecosystems(4). While these studies have given us an appreciation for the complexity of microbial communities, our understanding of how these microbiomes function is only just beginning.

Within microbiomes, it is thought that microbial natural products (i.e. antimicrobials, siderophores and quorum sensing molecules), also known as specialized metabolites, may play a variety of roles ranging from mediators of cooperation to all out chemical conflict(5). As such, these molecules may shape the composition and/or spatial distribution of organisms in microbial communities. Recently, a number of studies have demonstrated that microbial interspecies interactions can trigger the expression of gene clusters for specialized metabolism that remain silent during growth in pure culture(6, 7). While these observations seem to imply that microbes do use these molecules to mediate interactions, they underscore a key deficiency in our overall knowledge of specialized metabolism: we do not understand why microorganisms make these remarkable molecules nor how they employ this chemical repertoire in their natural habitat.

To evaluate the ecological role(s) of these small molecules, we need model systems of intermediate complexity. This is because axenic culturing techniques fall short of mimicking key aspects of microbial habitats, while environmental samples are often too complex to be understood with molecular-level resolution. Ideal model systems will allow researchers to manipulate the microbial community and test hypotheses with statistical power in a controlled laboratory setting, while also capturing a measure of the complexity of the natural environment.

Several natural and synthetic microbiome systems have been developed to address questions surrounding succession, cooperation, and competition. For example, cheese rind(8) and oral biofilms(9) are outstanding models for understanding community succession. Other host/microbiome systems, e.g. bobtail squid-*Vibrio*(10), mammal gut(11) and plant rhizosphere(12) are proving that systems once studied from a host-microbe perspective are valuable from a microbiome perspective as well. Other host systems have been studied in light of the specialized metabolic potential of their actinomycete symbionts, e.g. insects (13) and marine invertebrates(14), although manipulating microbes in these systems at the genetic level remains a key challenge. In order to answer key questions about microbial chemical ecology, we need ecologically-relevant model systems of intermediate complexity that lend themselves to experimental manipulation at the molecular level(15). In this chapter, we consider criteria for such model systems generally, and for examining the ecology of specialized metabolism, specifically.

1.2 Criteria for ideal model ecological systems

We view several elements as essential for maximizing the benefit of building model microbiome systems. However, the overarching consideration is that the model system should enable the testing of predictions originating from community ecology and evolutionary biology, while also enabling mechanistic questions to be addressed through genetic manipulation. Of course, all models are approximations and none are perfect, but we suggest that the five criteria we outline below may form the beginning of a guide for identifying natural systems of intermediate complexity that may form the bases for ideal microbiome models. In most cases, we imagine that these microbiome systems will be associated with host organisms, and thus we see the host as an integral part of the model system.

(i) The model should be based on a natural system: In our view, beginning with a natural microbial community maximizes the likelihood that the interactions we study will be relevant from a real-world perspective. Beyond this, recurring contact between organisms of different species is generally thought to be a prerequisite for co-evolution, and for cooperation(15). Thus, building a system with microbes that have routinely encountered each other over evolutionary time may diversify the types of interactions observed within the system.

(ii) The natural system should contain a relatively simple microbial community. Most habitats harbor microbial communities with very high species diversity and functional complexity. The mammalian gut and soil are key examples, and while these are among some of the most important systems from a human perspective, their complexity makes them refractory to reductionist experimental regimes. However, other host-associated microbiomes contain communities with a range of complexities. Hosts themselves apply selective pressures that may ultimately define simplified communities relative to microbiomes in environments such as soil. Examples of such host-microbiome communities include the Hawaiian bobtail squid(10), gut communities of nematodes(16) and insects (fruit flies (17) and honeybees(18)), and endophytic root communities(19). Choosing the members that will compose the model community is challenging to do without introducing experimenter bias. For this reason, we favor approaches based on host selection, wherein a natural community can be passaged through its host across several iterations(19). Doing so allows the host to select a reduced community and avoids bias introduced by rational criteria such as phylogeny or functional traits. It is expected that this methodology will afford the simplest functional community to a given host.

(iii) The model system should have an easily detectable output that indicates healthy microbiome function. In cases where the model microbiome is associated with a host organism, an overall indicator of microbiome function might be easily measurable host phenotypes, such as enhanced growth, pathogen resistance, or other indicators of stress. In cases where there is no associated host, the output can be based on functional outputs of the microbial community (like metabolic processes) that can be measured directly, as well as community dynamics and metabolomic, transcriptomic, and proteomic pattern analyses. All of these outputs are relevant when com- paring the model system with the natural environment, potentially allowing a measure of its ecological relevance.

(iv) The model system should contain microbial members that are culturable and genetically tractable. Ultimately, a model system must allow for strains with targeted mutations to be substituted for wild-type strains within the community, allowing hypothesis testing at the granular level of genes. Thus, a model system must contain organisms that are both culturable and genetically tractable, with a particular emphasis on keystone species. While genetic manipulation can be challenging, new techniques for genome editing via CRISPR-Cas9 (clustered regularly inter- spaced short palindromic repeats with Cas9)(20) and Argonaute(21) offer new opportunities in this regard. Finally, having genome sequences of all community members is key in terms of providing insights regarding the competence of the members and in facilitating targeted genetic analyses.

(v) The model system should be readily recapitulated in a laboratory setting and scalable. An ideal model system must be amenable to repeated iteration in a laboratory setting. To fully maximize this aspect of the model, the community should reproducibly reassemble, and the host-community system should be physically small and easily recapitulated on an order of tens to thousands to allow high-throughput interrogation. Moreover, easy reproducibility is essential to allow for quantitative/ statistical analyses.

It is unlikely that any single natural system can meet all of the criteria above, but many candidate systems might meet a subset of these criteria. This leads to an important question as researchers seek to evaluate different potential model systems: How can we tell if the model system captures important features of the natural system? This question is closely tied to the third criterion, wherein we suggest that an easily detectable indicator of microbiome health is ideal. In our view, a strong model microbiome will contain the minimum number of strains needed to recapitulate broad patterns seen in the natural system, while meeting as many of the criteria described above as possible.

The above criteria are meant as general considerations for any model microbiome system.

However, additional criteria might be considered for models to address specific ecological questions. For example, given our interest in the ecology of specialized metabolites we add the following.

(i) Microbially produced specialized metabolites should be detectable *in situ*. Since we seek to understand how specialized metabolites function in microbial com- munities, we view the ability to detect these molecules *in situ* as a critical aspect of a model system for chemical ecology. Thus, a key step is prior metabolomic investigation to assess the chemical diversity associated with a potential system. Emerging analysis techniques such as molecular networking and chemical dereplication(22) can help researchers rapidly assess such chemical diversity and identify potentially important specialized metabolites with more speed and accuracy than ever before. While measurement of specialized metabolites in natural habitats has been difficult historically, new tools such as mass spectrometry imaging (MSI) and nanospray desorption ionization (nano-DESI) mass spectrometry are providing new opportunities in this regard (23). Beyond this, combining MSI and microscopy will be essential to understand the spatial structure of the community and how it is affected by specialized metabolites.

(ii) The model community should possess robust specialized metabolic potential. Once the chemical diversity of a potential system has been evaluated, an important goal is to

capture as much of the chemical diversity as possible through inclusion of key community members that contribute to this diversity. This can be achieved based on culturing approaches, where isolates are grown under different conditions— ideally as similar as possible to the natural setting. The chemical profiles of these cultures can then be mapped against the molecular network obtained by the *in situ* analysis. This approach allows for inclusion of isolates that contribute the most to the specialized metabolite diversity detected *in situ*. Alternatively, the specialized metabolic potential could be assessed through genome sequencing of the isolates followed by genome-level analysis using tools like PRISM (24) and antiSMASH (25). Understanding the metabolic profile of the natural environment and how it changes over time will give valuable insights into the chemical ecology of the microbial specialized metabolism. The correlation between community dynamics and metabolomic patterns over time will be key to understanding how these molecules function in microbial communities.

As microbiome science progresses, the development of model microbiome systems that retain the key features of natural communities will be essential for elucidating the factors that dictate microbiome function. The criteria we outline here are aimed at developing model systems that will enable hypothesis testing at the genetic level and interpretation of results in the context of ecological and evolutionary theory. In turn, these results will enable the construction of predictive frameworks that will set the stage for rational manipulation of microbial communities associated with human health, agriculture, and industry. In this work, we propose the root nodule as a model for studying specialized metabolism in a simplified microbiome.

1.3 The root nodule as a model

The model organism *Medicago truncatula* (clover), has served as a model for both root microbiome(26) and root nodule studies (27). The root nodule is a symbiotic structure that forms on the roots of leguminous plants in the absence of bioavailable nitrogen and in the presence of nitrogen-fixing rhizobia. The clover root nodule model has allowed for a deep dive into the genetic drivers of this symbiosis and the development of in-laboratory nodulation techniques(28). In addition, sequencing and isolation efforts have revealed that the clover root nodule(26), alfalfa root nodule(29) and others(30) contain non-rhizobia. For example, Xiao and colleagues sequenced bulk soil, rhizosphere, endophyte and root nodule communities. Through this work they found a filtering effect in alfalfa that was also observed by Brown and colleagues in clover(26, 29). The simplification of this community across rhizo-compartments with the simplest natural root community existing in the root nodule makes this an interesting candidate microbiome to study due to its limited complexity.

Microbially-produced specialized metabolites, i.e. antibiotics, siderophores, and signaling molecules, drive interactions between microbes(31). Isolates from the root nodule have demonstrated specialized metabolite potential *in vitro*(30) however it is unclear if these compounds are produced *in planta*. With current model microbiomes and their respective limitations, the simple root nodule microbiome (relative to rhizosphere and bulk soil) with antibiotic potential presents as an interesting model to evaluate the role antibiotics play in mediating social interactions.

1.4 Concluding Introductory Remarks

In this work we sought to develop a simplified, defined root nodule microbiome derived from the root nodule of alfalfa in order to study microbial interactions driven by specialized

metabolites. The root nodule of alfalfa is a (i) a natural system, (ii) contains a relatively simple community, (iii) has an easily detectable output, (iv) contains members that are genetically tractable and culturable, and (v) is scalable to a laboratory setting. In addition, this model has the potential for (i) detection of specialized metabolites *in situ* that we later prove in through this work and (ii) has robust potential for discovery.

In order to develop this model, in chapter 2, we surveyed an agricultural field and evaluated the root nodule communities present using a 16S amplicon sequencing approach. We then developed a plant-based selection method to arrive at a simplified root nodule community that we could manipulate in the lab. We isolated four non-rhizobial members (*Brevibacillus brevis, Pantoea agglomerans, Pseudomonas sp*. and *Paenibacillus sp.)* and evaluated the interactions between all members in all possible combinations in the context of the root nodule and through *in vitro* assays. In taking this approach we discovered both positive and negative interactions exist depending on co-inoculation partners. *B. brevis* stood out as a dominant member with antagonistic behavior capable of disrupting cooperative interactions.

To follow up this work and identify specialized metabolites that may be driving these interactions, in Chapter 3, we took a metabolomics approach paired with a multi-Venn analysis to identify important compounds within this system. This analysis paired with MALDI imaging mass spectrometry allowed us to describe the spatial structure of this root nodule community. In addition, the metabolomics/Venn approach also led us to the discovery that *B. brevis* produces a known antibiotic, Tyrocidine A, and one novel antibiotic, Britacidin A, *in planta*. We then sequenced the genome and described the gene cluster responsible for Britacidins. In doing so, we demonstrated that non-rhizobia are metabolically active in the root nodule and that this approach is a viable option for evaluating community interactions mediated by specialized metabolites.

Chapter 2: Characterization of a synthetic root nodule microbiome in Alfalfa

A portion of this chapter has been adapted from the following with permission:
Hansen, B.L., Pessotti, R.C., Fischer, M.S., Collins, A., El-Hifnawi, L., Liu, M.D. and Traxler, M.F. (2020) Cooperation, Competition, and Specialized Metabolism in a Simplified Root Nodule Microbiome. mBio. 11(40) e01917-20. doi: 0.1128/mBio.01917-20

2.1 Introduction

Plants harbor distinct microbial communities associated with their roots(32–34), stems(33–35), leaves(33–36), and flowers(37, 38). These communities can influence host phenotypes in a variety of ways that are beneficial, including enhanced growth(37, 39), drought tolerance(33, 34, 40), and disease resistance(33, 34, 37). The content of these microbiomes is thought to be shaped by a combination of historical contingency (i.e. the order of strain arrival)(41), microbial interspecies interactions(19, 42), and nutrients or other compounds exuded by the plants themselves that may select for microbes with beneficial characteristics(2, 43). Specialized metabolites produced by microbes, including molecules with antibacterial, antifungal, and siderophore activities, have been hypothesized to play a role in shaping plant microbiomes. For example, specialized metabolites may influence interactions between members of plant microbiomes(44–46), and be a mechanism of protection from pathogen invasion(38, 46). Thus, there is interest in leveraging specialized metabolism by plant-associated microbes in agriculture, and for novel compound discovery.

Legume plants are notable from a microbial perspective because they form specialized, N-fixing organs, called nodules, through intimate association with bacterial symbionts of the orders Rhizobiales and Burkholdariales. Biological N-fixation by legumes plays a significant role in the global N cycle, with estimates ranging from 39-70 Gg of N fixed per year on a global scale(47, 48). Owing to the agricultural and ecological importance of N-fixation, this plant-microbe symbiosis has been the subject of intense research for several decades(49–60). As a result, much is known about the genes and chemical signals and molecular mechanisms that underpin this symbiosis(49, 61–63). While nodulation has traditionally been studied as a two-member system, more recently it has become clear that root nodules harbor an accessory microbiome(64–68). In a recent study, Xiao and co-workers found that the different rhizo-compartments of *Medicago sativa* (i.e. the rhizosphere, root endosphere, and nodules) were successively limited in microbial diversity, with the nodule containing the simplest community(65).

Several lines of *in vitro* evidence suggest that members of the nodule microbiome may be a rich source of specialized metabolites. For example, a novel antibiotic, phazolicin, was described from a *Rhizobium sp*., isolated from the root nodules of *Phaseolus vulgaris* (wild beans)(69). Additionally, *Micromonospora* and *Paenibacillus sp*. isolated from the root nodules of *M. sativa,* showed antifungal activity against common phytopathogens *in vitro*(64, 70–72). The relative simplicity of the nodule microbiome, and the observation that members of this microbiome have potential for specialized metabolism, make the nodule an attractive system for exploring microbial interactions and the ecological roles of specialized metabolites *in situ*. With this in mind, we sought to develop a tractable nodule microbiome system: 1) whose members were derived from field-grown plants, 2) that was easily experimentally manipulated, and 3) that enabled interrogation of the system at the chemical level. Here, using a combination of community profiling and a simplified nodule community, we report that the *M. sativa* root nodule microbiome is dynamic

over time and life phase, the nodule microbiome contains members that strongly interact through cooperation and competition, and that microbes within the nodule community produce specialized metabolites. Taken together, these results lend support to the idea that in addition to nitrogen fixation, legume root nodules may be sites of active antimicrobial production. A possibility we explore further in Chapter 3.

2.2 Results

2.2.1 Community profiling across root nodule development

Here we sought to develop an experimentally tractable root nodule microbiome system using *Medicago sativa* (alfalfa). This legume was chosen since protocols are readily available for its gnotobiotic germination and nodulation(28), and the plants are small enough to enable good scalability for experiments requiring many replicates. Beyond this, alfalfa is of interest from an agriculture perspective, being the fourth most widely grown crop in the United States(73).

Over the last decade, non-Rhizobiales members of nodule microbiomes have previously been detected in root nodule tissue(65). However, it is unclear if these bacteria are present across the lifetime of individual nodules. We define three developmental phases of the alfalfa root nodule; young nodules (small and white), active nodules (pink/red), and senescent nodules (brown/green coloration) (Fig. 1A). The pink color in active nodules is due to the presence of leghaemoglobin, whereas the brown/green color during senescence is due to the degradation of the heme group associated with leghemoglobin(74). To address whether or not the nodule microbiome varied across these phases, we harvested nodules from established alfalfa plants (~10 years) from an agricultural field in Alturas, California. We classified each nodule as young, active, or senescent, extensively washed their outer surfaces and extracted DNA for 16S amplicon sequencing (SRA accession: PRJNA608732).

We found that an accessory community was present throughout the nodule life cycle (Figure 1B) and the relative abundance of this community differed between developmental stages. For instance, *Ensifer* (Proteobacteria) made up 94-96% of the operational taxonomic units (OTUs) in young nodules and active nodules, but its relative abundance was reduced to ~86%, in senescent nodules. Representatives of the genus *Pseudomonas* had an average relative abundance of 2.45% in young nodules, however they decreased to 0.03% and 0.05% in active and senescent nodules, respectively. Conversely, the actinobacterial taxa *Streptomyces*, *Actinoplanes,* and *Micromonosporaceae*_unclassified all increased from ~0.1% in young nodules to ~1.60% in senescent nodules. TM7 is a phylum thought to be associated with Actinobacteria, and it also increased across these developmental stages from 0.06% to 0.10% and 5.70%. Similar relative abundance changes captured across root nodule development were observed in *M. sativa* grown in varying soil conditions (Supplemental Fig. S1, all supplemental items can also be found at https://doi.org/10.6084/m9.figshare.12107094). Collectively these results indicate that the root nodule microbiome is both simple and dynamic as nodules mature from young through active and senescent phases.

2.2.2 Root nodule microbial community selection

The agricultural root nodule microbiome has been described as having considerably less richness relative to the root and surrounding bulk soil(65, 66, 75, 76). This simplicity prompted us to consider if we could develop an experimentally tractable nodule microbiome system(77). In order to do this, we used *in planta* selection to arrive at a simplified bacterial community. We started

with agricultural nodules from all three developmental phases, surface sterilized them, and homogenized them to obtain a comprehensive inoculum. This homogenized material was re-suspended in sterile water and inoculated onto the roots of gnotobiotic three-day-old *M. sativa* seedlings. These seedlings were also inoculated with *Sinorhizobium meliloti* RM1021, the well-studied, nodulating symbiont of *M. sativa*. We grew these plants under controlled conditions for 3-5 weeks and harvested root nodules from all three phenotypic stages for parallel 16S community profiling (SRA accession: PRJNA608732) and bacterial isolations. Nodules from all three phenotypic stages were once again surface sterilized and homogenized to obtain the inoculum for the next passaging round (Fig 2A). We repeated these steps three times and arrived at a final simplified community comprised of four accessory bacterial members: *Brevibacillus brevis* Ag35, *Paenibacillus sp*. Ag47, *Pseudomonas sp*. Ag54, *Pantoea agglomerans* Ag15, plus the nodulating strain, *Sinorhizobium meliloti* RM1021 (Fig 2B & Supplemental Table S1).

Figure 2B shows that the four members of this community rose to prominence in the accessory microbiome relatively quickly during the first round of passaging and continued to dominate the accessory community through the second and third passages. These data indicate that this accessory community is the product of relatively strong selection in our gnotobiotic nodule system. We note that OTUs representing each of the four accessory members of this community were detected in our initial 16S community profile from field-grown nodules, and that members of each of these taxa have been found as members of the nodule microbiome in other studies(29, 64, 78). Inoculation with this community did not affect plant height or nodule number relative to control plants (Supplemental Fig. S2A&B).

2.2.3 *In planta* community assembly and recoverability

Given that the relative abundance measurements in Figure 2B represent the average community across ten nodules, we sought to assess colonization/maintenance of the accessory community at the level of individual nodules. To do so, we combined the gnotobiotic alfalfa system with a culture-based approach to assess the recovery rate (i.e. the percentage of nodules containing a given bacterial strain) of each community member. First, we inoculated each microbe alone on three-day old seedling roots and found that each microbe was insufficient to generate nodules (Supplemental Figure 2), as expected. We next set up a series of experiments in which each microbe was co-inoculated with the nodulating strain, *S. meliloti* RM1021. For these accessory community experiments, unless otherwise noted, *S. meliloti* RM1021 was always included. Two out of the four accessory community members were recoverable from active root nodules when they were the sole accessory community member, *Brevibacillus brevis* Ag35 (recovery rate of 40%) and *Paenibacillus sp*. Ag47 (64%). The individual recovery rates where highly variable for each microbe when co-inoculated in combination with other accessory members, as summarized in Fig 3A and Supplemental Table S2&3.

Within these combinations, examples of ecological cooperation and competition, as defined by Mitri *et al*(15) were apparent (Figure 3B, Supplemental Fig S3 & Supplemental Table S6). For example, *Pseudomonas sp*. Ag54 was unrecoverable (0%) when it was the sole accessory community member from all fifteen nodules assayed (Figure 3B). However, when we added *Paenibacillus sp*. Ag47 and *Pseudomonas sp*. Ag54 (together with *S. meliloti)*, we observed each member's recovery rate increased to 83% (Figure 3A) and eight out of 12 nodules contained both members (Figure 3B), with zero nodules lacking at least one of these strains. This represented a 20% increase for *Paenibacillus sp*. Ag47, and a striking 83% increase for *Pseudomonas sp*. Ag54.

This positive interaction changed when we added *B. brevis* Ag35 (highlighted in Figure 3B). When all three microbes where included, the recovery rates of *Paenibacillus sp.* Ag47 and *Pseudomonas sp.* Ag54 decreased by ~66% and ~72%, respectively, compared to when they were inoculated as a pair. Thus, the addition of *B. brevis* Ag35 abrogated the benefits of cooperation observed between *Pseudomonas sp.* Ag54 and *Paenibacillus sp.* Ag47. This negative impact indicates that *B. brevis* Ag35 shifted the community into a mode driven by competition, rather than cooperation.

We noted that while the observed cooperation between *Pseudomonas sp.* Ag54 and *Paenibacillus sp.* Ag47 was evident in terms of recovery rate, in terms of abundance of each partner, i.e. colony forming units (CFU), the results were complex (See Supplemental Table S6 and Supplemental Fig. S17). *Pseudomonas sp.* Ag54 was unrecoverable (0 CFU/nodule) when inoculated with *S. meliloti* RM1021 alone, however, when co-inoculated with *Paenibacillus sp.* Ag47, the average CFU increased to ~65 CFU/nodule. Interestingly, when *Paenibacillus sp.* Ag47 was co-inoculated with only *S. meliloti* RM1021, it had an average CFU of ~280/nodule, however, when co-inoculated with *Pseudomonas sp.* Ag54, this number deacreased by ~4 fold (~69 CFU/nodule). This negative effect was unexpected given the enhanced recoverability of *Paenibacillus sp.* Ag47 with the addition of *Pseudomonas sp.* Ag54. These data indicate that microbial interactions can have disparate effects on different aspects of life in root nodules. In this example, *Pseudomonas sp.* Ag54 and *Paenibacillus sp.* Ag47 may be cooperative during the nodule colonization process (affecting recoverability) yet result in a cost for *Paenibacillus sp.* Ag47 at the level of average abundance over time.

2.2.4 Bioactivity of accessory community members

Several studies have observed that bacteria isolated from root nodule tissue can frequently make bioactive compounds *in vitro* (See (64) for a comprehensive review). Therefore, we hypothesized that the outcomes we observed in our *in-planta* experiments could be due to antibiotic-mediated interspecies interactions. To address this possibility, we grew each microbe on medium designed to mimic nutrients available within nodules (described in materials and methods, hereafter referred to as 'root nodule medium') and assayed each microbe's inhibitory activity against lawns of all the other community members. We found that all accessory members had inhibitory activity against one or more members, and all members inhibited *S. meliloti* RM1021 growth (Figure 3C). We used the outcome of this assay in tandem with the outcomes of the *in-planta* experiments to produce a summary map for interactions within this simplified community (Figure 3D).

2.3 Discussion

The root nodules of legume plants play host to a relatively simple associated microbiome(64). Several studies have provided examples of microbes isolated from root nodules that produce antimicrobial compounds *in vitro*(64, 71). These observations prompted us to consider legume root nodules as systems that might be, 1) ideal for development as simplified experimental microbiome for exploring interactions mediated by specialized metabolites, and 2) fruitful in terms of novel compound discovery.

Multiple studies have used 16S amplicon sequencing to profile root nodule communities, including those of *Medicago sativa*(65), *Lotus japonicus*(66), and *Glycine max*(75). Across these studies, the major phyla that were consistently observed as nodule-associated included Actinobacteria, Proteobacteria, and Firmicutes. The work of Xiao and co-workers has shown this community to be relatively low diversity compared to the rhizosphere or root endophyte

communities(65). In this work, we began with nodules from alfalfa plants from an agricultural field in Alturas, California. We separated nodules based on whether they were young (small with no pink coloration), active (based on heme/pigmentation presence), or senescent (based on the presence of oxidized leghemoglobin) and asked if the microbiome varied across these phases.

Not surprisingly, the nodule community was dominated by Rhizobia at all phases, however, we found that the progression from young to active to senescent was accompanied by an overall increase in non-rhizobial relative abundance. This result parallels observations made in the 1970s and before that older nodules tended to have abundant 'contaminants' that complicated the straightforward isolation of the symbiotic *Rhizobiales*(79). One possible explanation is that the increased bacterial richness in nodules as they progress toward senescence indicates increased potential for latent saprotrophy. Alternatively, older nodules may simply have had more time to acquire a diverse microbial community. Across this progression, we also observed an increase in the relative abundance of Actinobacteria and TM7, whose members are thought to be broadly associated with Actinobacteria as epibionts(80). In contrast, we found that Proteobacteria and Bacteroidetes had a general decrease in relative abundance across these stages. Finally, Firmicutes make up a very small fraction of the community but their relative abundance did not fluctuate. Overall, these results indicate root nodules have a microbial community that is dynamic across root nodule developmental phases, and thus, we suggest that future studies take these phases into account when proceeding with isolations or community analyses. Beyond this, we note that the finding that the nodule microbiome shifts with these phases reinforces the conclusions of Edwards and co-workers(81) who showed that a key driver of root endosphere community structure was the developmental stage of the host plant.

To begin characterizing the functional relationships between members of the root nodule microbiome, we sought to develop a simplified, tractable nodule microbiome system that was amenable to experimental manipulation *in planta*. We took a similar approach to that of Niu and co-workers(19) in which the plant itself was used to select a simplified endophyte community. To do so, we started with crushed root nodules from mature agricultural alfalfa plants and applied this inoculum to a gnotobiotic system containing alfalfa seedlings and *Sinorhizobium meliloti* RM1021. After three rounds of passaging, the accessory nodule community contained just four culturable species, *B. brevis, Paenibacillus sp., P. agglomerans,* and *Pseudomonas sp.*. These four bacterial species were present in the original 16S community profiles of the agricultural nodules although at very low relative abundance. However, after just two rounds of passaging through root nodules, these four bacterial species dominated the community, suggesting this simple community is the result of relatively strong selection within this system. The selection pressures in such a gnotobiotic system undoubtedly vary from the complex environmental conditions found in the field. One key difference may include a strong pressure to thrive on root exudates in an artificial environment. Additionally, soil structure, soil nutrients, and the continued presence of the surrounding soil microbial community, which are absent in our gnotobiotic system, may influence the microbiome across the nodule life cycle. However, the four bacterial species that comprise this community have also been reported as associated with root nodules from a variety of legumes(64, 72, 75, 82–84), indicating that these microbes are frequently found in natural root nodule accessory communities.

The simplicity of this community allowed us to reconstruct it in every possible combination *in vitro* and *in planta*. This enabled us to see each member's impact on the other members of the community and demonstrated complex examples of cooperation and competition among them. For example, *Pseudomonas sp*. Ag54 was not recovered from nodules when inoculated as the sole

accessory community member, however, it was frequently recovered when other community members were also included. When *Pseudomonas sp*. Ag54 and *Paenibacillus sp*. Ag47 were co-inoculated, *Pseudomonas sp*. Ag54 was recovered from greater than 80% of the nodules. This pairing was also beneficial for *Paenibacillus sp*., whose frequency also increased in the co-inoculated nodules. The mutual benefit observed in this interaction is a notable example of *in planta* cooperation among members within this community. We note that while this cooperation was apparent in terms of the recoverability of both organisms, the average abundance (CFU) of *Paenibacillus sp*. Ag47 decreased with the addition of *Pseudomonas sp*. Ag54. These results lead us to hypothesize that relationships between microbes likely shift during different processes or nodule life phases. For example, *Paenibacillus sp*. Ag47 and *Pseudomonas sp*. Ag54. may cooperate during nodule colonization (boosting the recovery rate of both) but develop a competitive relationship as they persist over time within nodules (having a negative effect on *Paenibacillus sp*. Ag47 average abundance).

Intriguingly, when *B. brevis* Ag35 was co-inoculated with *Pseudomonas sp*. Ag54 and *Paenibacillus sp*. Ag47, both *Pseudomonas sp*. Ag54 and *Paenibacillus sp*. Ag47 showed reduced recovery rates compared to when they were inoculated as a duo, and *B. brevis* Ag35 showed reduced recovery compared to when it was inoculated as the sole accessory community member. This dynamic indicates that the benefit of cooperation between *Pseudomonas sp*. Ag54 and *Paenibacillus sp*. Ag47 was insufficient to counteract the negative effect of competition with *B. brevis* Ag35. Such cooperative interactions, and their disruption through competition, are ideal for further exploration at the mechanistic level. Beyond the accessory community interactions, it is important to consider how the community members impact the nodule symbiont. As seen in Figure 3C, each accessory community member appears capable of antagonism against *S. meliloti*. Therefore, follow-up studies should aim to assess the impact these members on the rhizobial symbiont *in planta* with specific focus on assessing how the accessory microbiome may influence total nitrogen fixation.

2.4 Materials and Methods

2.4.1 Collection of agricultural *Medicago sativa* from Alturas, Ca

M. sativa plants were carefully sampled with roots and rhizosphere intact from Alturas Ranches, in Alturas, CA. The plants were transported for six hours at room temperature and subsequently rinsed with double-distilled water (ddH_2O) until visible soil particles from rhizosphere were removed.

2.4.2 Collection of soil from Hopland, CA and growth of Medicago sativa

Soil from Hopland, CA UC Berkeley Field station (39°00'14.6"N 123°05'09.1"W 39.004050, -123.085871) was collected for in lab growth experiments. The top 10-15 cm of soil was removed and 15-30 cm zone was collected (Niu B, Paulson JN, Zheng X, Kolter R. 2017. Proc Natl Acad Sci 114:e2450–e2459). and was stored at room temperature for 24 hours before use. Medicago sativa seed from Fisher science education (reorder code: S041368) was inoculated with 50 ml *Sinorhizobium meliloti* RM1021 GFP (Table S1) at an OD600 of 0.1. Seeds were planted 2 cm deep in 0.5-gallon pots. The plants were placed under T5 lights on a 16:8 light: dark cycle at ambient room temperature 25 ± 2 °C for six weeks until ready for harvest. Plants were watered via

a water reservoir tray. Root nodules were surface sterilized, environmental DNA (eDNA) extracted and 16S amplicon sequencing was performed as described in Methods.

2.4.3 Growing M. sativa at Oxford field tract in Berkeley, Ca

Medicago sativa seed was inoculated with 50 ml Sinorhizobium meliloti RM1021 at an OD600 of 0.1 and spread over a 2ft x 8ft plot at the Oxford Tract, UC Berkeley. 2 cm of soil was spread to cover the seed and watered for 60 minutes, 4 times a week for six weeks. Root nodules were surface sterilized, eDNA extracted and 16S amplicon sequencing was performed as described below.

2.4.4 Root sterilization and root nodule collection

The roots were surface sterilized with commercial bleach for 2 minutes, rinsed with filter sterilized ddH_2O and then transferred to 70% ethanol for 30 seconds. Roots were rinsed with sterile ddH_2O five times and the last rinse was concentrated and plated on tryptic soy agar (TSA) and International Streptomyces Project (ISP) #2 agar to check for full removal of surface bacteria. Surface sterilized root nodules were cut free from the plant at the base of the nodule using a sterile blade and sorted into three phenotype groups: young (white), active (pink/red) and senescent (dark green) as seen in **Figure 1A**. Nodules were pooled in groups of 10 and crushed using a sterile pestle gun in micro-centrifuge tubes for 30 seconds. Crushed nodules were re-suspended in 200 μL deionized water for further processing **(Figure 2A).**

2.4.5 Environmental DNA extraction and 16S rRNA amplicon sequencing

All root nodule samples were processed with the Powerplant Pro DNA extraction kit (Qiagen). Amplicon sequencing libraries were prepared by amplifying the V3-V4 region as described by Simmons et al(85) using Q5 Hot Start polymerase Master Mix. Polymerase chain reaction conditions were optimized for low eDNA yield by the following modification: annealing at 60 °C for 60 seconds. Paired-end sequencing was performed on the MiSeq at the QB3 facility (SRA accession: PRJNA608732). The data was analyzed using the Mothur MiSeq protocol and clustering was done using agc method(86) (Date accessed:10-05-2018) and phyloseq(87) with R v3.5.0 in R studio v1.1.447.

2.4.6 Passaging Experiment

We sterilized ~400 seeds by mixing them with ethanol for 30 minutes, removing the ethanol and then mixing the seeds with bleach for 30 minutes. Seeds were copiously rinsed five times with ddH_2O and then germinated on Jensen's agar(28) for 3 days at RT out of direct light (covered in foil). Plant microcosms were constructed as described by Jones *et al*(28) with modifications: 40 ml of Jensen's agar in 100x15mm plastic petri dishes. Root inocula prepared as follows: 50ul of crushed root nodule mixture containing young, active, and senescent nodules from Alturas, CA was diluted in 1 ml of sterile ddH_2O. *S. meliloti* at a final OD_{600} of 0.05 was added 1:1 to the mixture to ensure nodules form. Plants were grown in growth chambers constructed from sterilized germination trays with tall clear propagation domes that were sterilized with UV, bleach, and 70% ethanol prior to being used as a growth chamber. These trays were placed under 16:8 light:dark conditions at 25 ± 2 °C. Control plants were inoculated with either sterile water or *S. meliloti* at O.D. ~ 0.05. Root nodules were harvested at 21 days and used for the next passaging. Plants were measured and roots were sterilized using the same protocol above. 10 root nodules per sample x 3 samples x 3 phenotypes x 4 conditions = 36 samples per passage. Each passage, 15 microcosms

were constructed containing two plants per microcosm. The last passage harvest was conducted at 5 weeks to ensure full development of root nodules and 10 root nodules per sample x 5 samples x 3 phenotypes x 4 conditions samples were collected from this passage.

2.4.7 Bacterial Isolates

Root nodules from all conditions were crushed with a sterile pestle and re-suspended in 50ul sterile ddH_2O. Post-passaging isolations were performed from 50ul of a 200ul root nodule sample suspension. All 50ul samples from each condition and phenotype were pooled, and 10ul of a 1:2, 1:10 and 1:100 dilution were plated on the following media: International Streptomyces Project (ISP) 1, ISP2, ISP3, ISP5, ISP7, tryptic soy agar (agar 15 g/L, casein peptone 15 g/L, sodium chloride 5 g/L, and soya peptone 5 g/L), Potato Dextrose agar (Potato Starch 4g/L, Dextrose 20 g/L, and agar 15 g/L), SM3 (Dextrose 10 g/L, Peptone 5 g/L, Tryptone 3 g/L, Sodium chloride 5 g/L and agar 15 g/L), and SKM (Skim milk 10 g/L, Magnesium sulphate 0.5 g/L and gelzan 8 g/L).

2.4.8 Species Identification

Colony PCR was performed on isolates grown on ISP2 or LB for four days. One colony was added to 20ul ddH_2O, boiled for 10 minutes at 98C in a thermocycler. Then the cell debris was pelleted by centrifugation and DNA concentration was measured with a Nano-drop. 60ng of DNA was used as a template for PCR with the primers: 1492R (5'-GGTTACCTTGTTACGACTT-3') and 27F (5'-AGAGTTTGATCCTGGCTCAG-3') to amplify the 16S gene and BLAST for genus identification.

2.4.9 Microcosm experiments with selected accessory community

Sterilized seeds by mixing them with ethanol for 30 minutes, removing the ethanol and then mixing the seeds with bleach for 30 minutes. Seeds were copiously rinsed five times with ddH_2O and then germinated on Jensen's agar(28) for 3 days at RT out of direct light (covered in foil). Plant microcosms were constructed as described above. Root inocula prepared as follows: Bacteria were grown on Lennox LB for 24 hours, a colony was subsequently picked and re-suspended in ddH_2O, and the OD_{600} taken. Bacteria were added at an OD_{600} of 0.05 in a 1:1 ratio at a final volume 200ul per microcosm to ensure the same number of cells were added of a single bacterium across conditions. Plants were grown in growth chambers constructed from UV, bleach and 70% ethanol sterilized germination trays with tall clear propagation domes. These trays were placed under 16:8 light:dark conditions at 25 ± 2°C. Control plants were inoculated with either sterile water or *S. meliloti* at O.D. ~ 0.05. Root nodules were harvested at 14 days. Plants were measured and roots were sterilized using the same protocol above. Roots were sterilized with 30s bleach, 45s ethanol, rinse 5x water and root nodules were removed with sterile blade and forceps.

2.4.10 Bioactivity agar-plug diffusion assay

Each bacterium was grown on Root nodule medium for three days in triplicate at 30°C. An agar plug from each plate of bacteria was placed on a fresh lawn of each bacterium and incubated at 30°C overnight. The presence (a clearing) or absence (bacterial growth around the agar plug) was recorded.

Chapter 2 Figures

Figure 1. 16S community profiling of three different root nodule developmental phenotypes from agricultural *M. sativa* plants. (A) Images of young (Y, white), active (A, pink/red) and senescent (S, brown/green) nodules. (B) Relative abundance of each phyla based on 16S-amplicon sequencing of young, active and senescent root nodules from an agricultural field in Alturas, Ca. (C) Relative abundance of each phyla excluding Rhizobia.

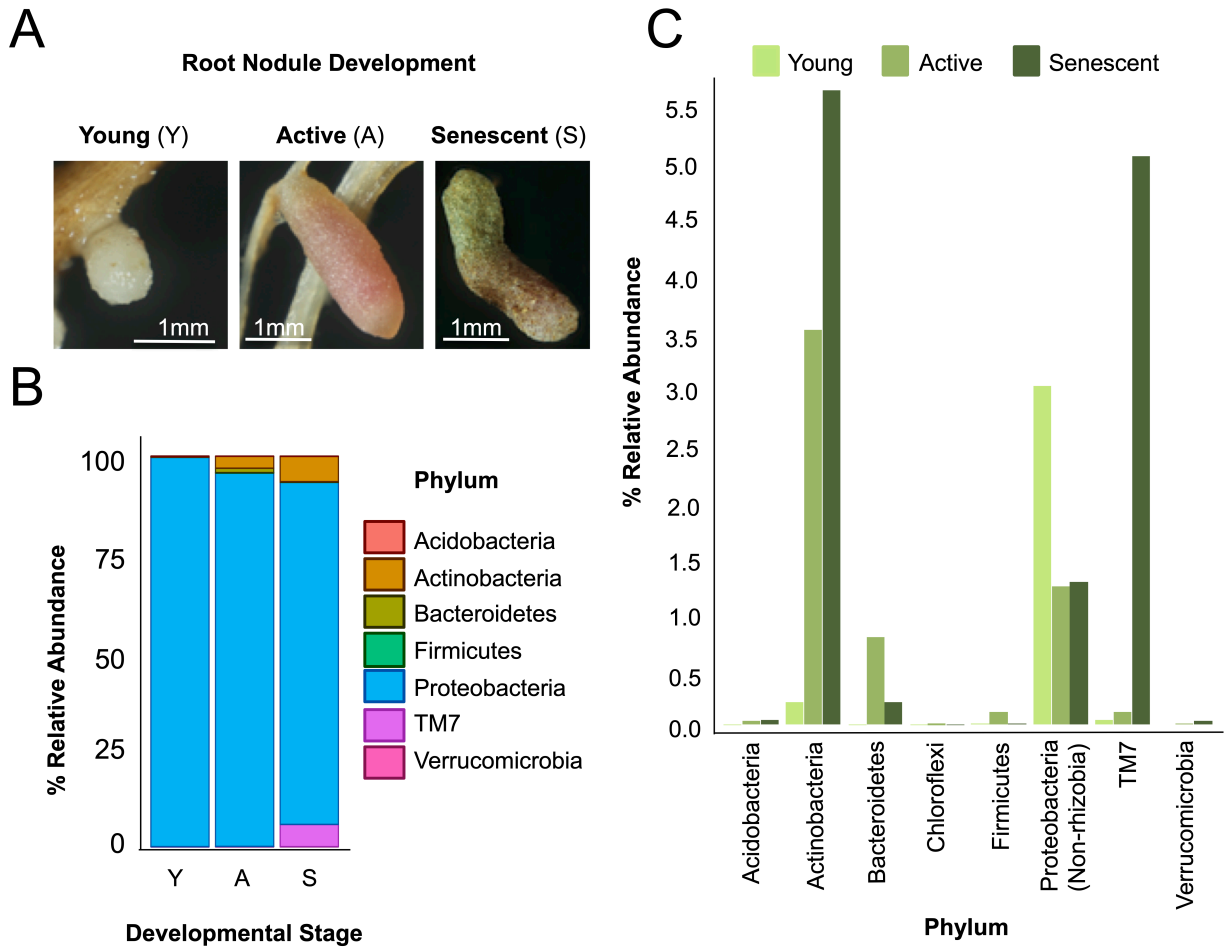

Figure 2. Root nodule microbial community selection with *M. sativa*. (A) Schematic showing the workflow for creating the microbial community; Step 1) Crushed nodules were inoculated onto gnotobiotic plant roots. Plants were incubated until nodules formed and then, Step 2) roots were surface sterilized and nodules removed and sorted based on phenotype. Step 3) Nodules were crushed and re-suspended in water. This homogenous mixture was used for three applications; to repeat the process by applying to gnotobiotic roots (Step 4a), environmental DNA extraction for 16S amplicon sequencing (Step 4b), and for isolation of bacteria (Step 4c). (B) Relative abundance of non-*Ensifer* operational taxonomic units (OTUs) at the genus level from each successive root nodule inoculum ("round") across root nodule phenotype. Black boxes indicate genera isolated after Round 3 and used for subsequent experiments.

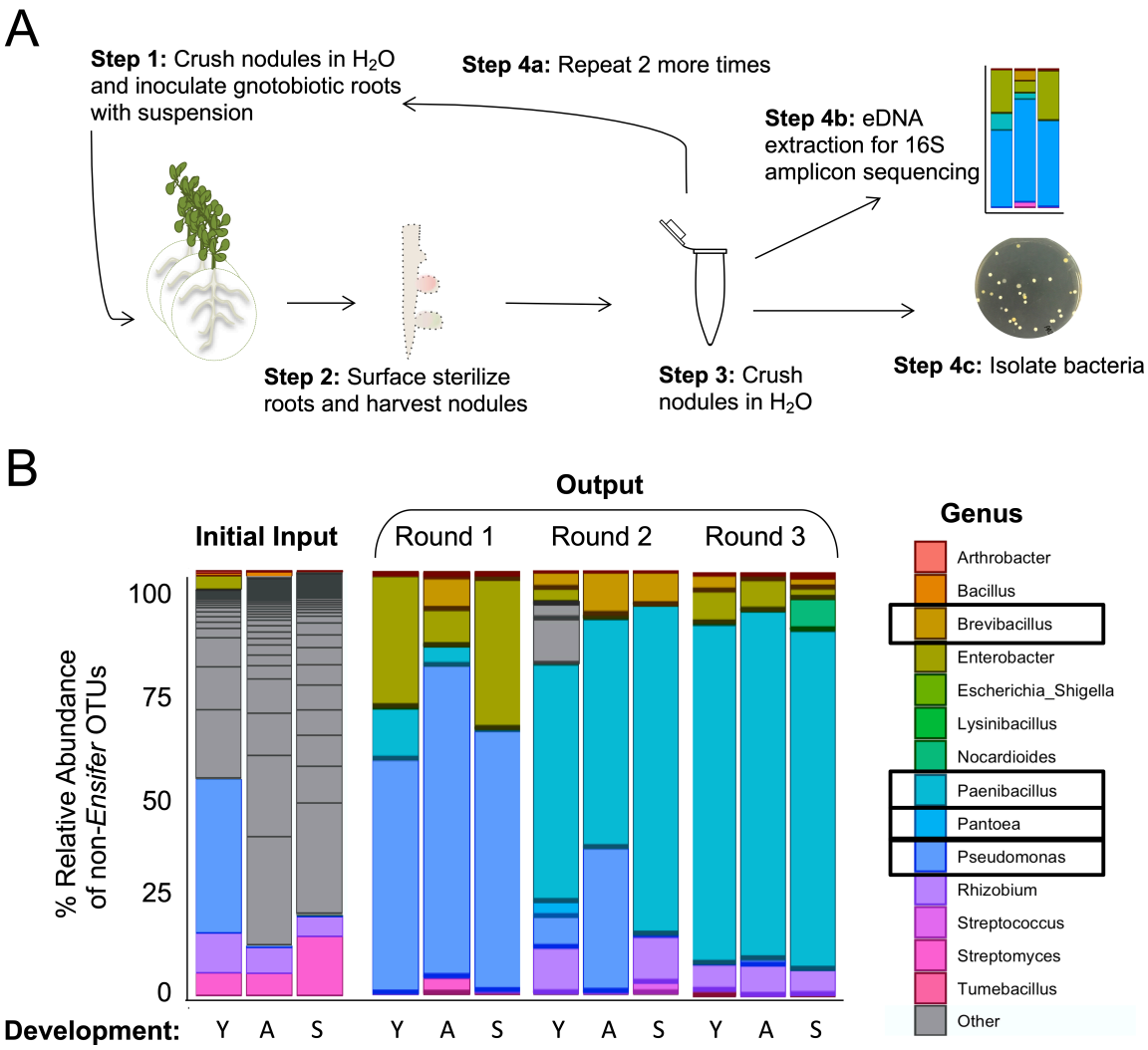

Figure 3. Interactions between members of the synthetic root nodule community. (A) Rate of re-isolating (or, recovering) each bacterium from *M. sativa* roots that were inoculated with the bacterial isolates that resulted from the selection process detailed in Figure 2. Experimental treatments were all possible combinations of these bacteria inoculated onto *M. sativa* roots with the essential nodulation strain; *S. meliloti*. These plants were grown until they developed root active nodules, and then bacteria were systematically re-isolated from these root nodules. Recovery rates for each bacterium are relative to the recovery rate from plants that were inoculated with one bacterium plus *S. meliloti*. White boxes indicate bacterium was not added to inoculum. Grey (zero change), blue (negative relative recovery) and yellow (positive relative recovery). (B) The number of bacterial colonies recovered from treatments 12, 9, 15, and 4 (see figure S3 for all other treatments). Numbers within grey circles labeled "None" represent the number of nodules where no bacterium was recovered, while numbers in colored circles represent the number of nodules where one or more bacteria were recovered. (C) Bioactivity agar-plug diffusion assay of each member against a lawn of each member on root nodule agar medium. Red squares indicate a zone of inhibition was observed and tan squares indicate no inhibition zone was observed. (D) Model summarizing the interactions observed for microbe recovery *in planta* (A and B) and *in vitro* (C).

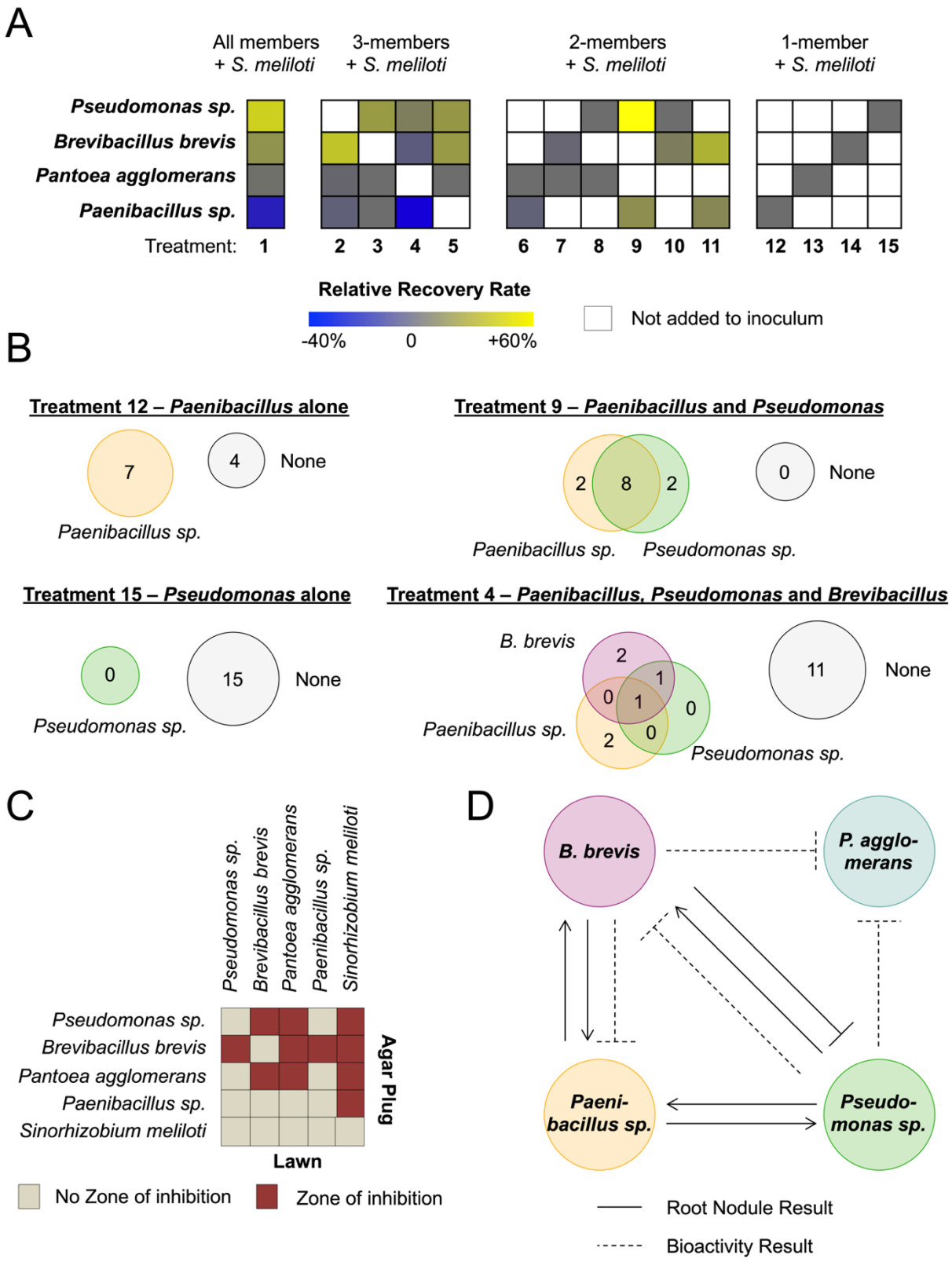
A
All members + S. meliloti
3-members + S. meliloti
2-members + S. meliloti
1-member + S. meliloti
Pseudomonas sp.
Brevibacillus brevis
Pantoea agglomerans
Paenibacillus sp.
Treatment: 1 2 3 4 5 6 7 8 9 10 11 12 13 14 15
Relative Recovery Rate
-40% 0 +60%
Not added to inoculum
B
Treatment 12 – Paenibacillus alone
7
4
None
Paenibacillus sp.
Treatment 9 – Paenibacillus and Pseudomonas
2
8
2
0
None
Paenibacillus sp.
Pseudomonas sp.
Treatment 15 – Pseudomonas alone
0
15
None
Pseudomonas sp.
Treatment 4 – Paenibacillus, Pseudomonas and Brevibacillus
B. brevis
2
1
0
1
0
2
0
11
None
Paenibacillus sp.
Pseudomonas sp.
C
Pseudomonas sp.
Brevibacillus brevis
Pantoea agglomerans
Paenibacillus sp.
Sinorhizobium meliloti
Agar Plug
Lawn
No Zone of inhibition
Zone of inhibition
D
B. brevis
P. agglo-merans
Paeni-bacillus sp.
Pseudo-monas sp.
Root Nodule Result
Bioactivity Result

Chapter 2 Supplemental Tables

Table S1. Table of strains used in this study. Strains with strain IDs with an "Ag" prefix were isolated after gnotobiotic passaging as described in Figure 2.

Species	**Strain ID**	**Origin**
Pantoea agglomerans	Ag15	Alturas, CA – post passaging
Brevibacillus brevis	Ag35	Alturas, CA – post passaging
Paenibacillus sp.	Ag47	Alturas, CA – post passaging
Pseudomonas sp.	Ag54	Alturas, CA – post passaging
Sinorhizobium meliloti	RM1021 GFP	Cheng HP, Walker GC. 1998. J Bacteriol 180:5183–5191.

Table S2: Raw recovery values of each member across treatments for Figure 3A. Values represent the number of nodules where the bacterium was recovered / total number of nodules assayed.

Microbial Treatment	***Pseudomonas sp.* Ag47**	***Brevibacillus brevis* Ag35**	***Paenibacillus sp.* Ag47**	***Pantoea agglomerans* Ag15**
S. meliloti RM1021, Ag47	NA	NA	0.636	NA
S. meliloti RM1021, Ag15	NA	NA	NA	0.000
S. meliloti RM1021, Ag35	NA	0.400	NA	NA
S. meliloti RM1021, Ag54	0.000	NA	NA	NA
S. meliloti RM1021, Ag54, Ag35	0.000	0.500	NA	NA
S. meliloti RM1021, Ag35, Ag15	NA	0.375	NA	0.000
S. meliloti RM1021, Ag35, Ag47	NA	0.800	0.800	NA
S. meliloti RM1021, Ag15, Ag47	NA	NA	0.583	0.000
S. meliloti RM1021, Ag54, Ag47	0.833	NA	0.833	NA
S. meliloti RM1021, Ag54, Ag15	0.000	NA	NA	0.000
S. meliloti RM1021, Ag35, Ag15, Ag47	NA	0.903	0.581	0.000
S. meliloti RM1021, Ag54, Ag47, Ag15	0.273	NA	0.636	0.000
S. meliloti RM1021, Ag54, Ag35, Ag47	0.105	0.316	0.158	NA
S. meliloti RM1021, Ag54, Ag15, Ag35	0.250	0.667	NA	0.000
S. meliloti RM1021, Ag54, Ag35, Ag47, Ag15	0.570	0.570	0.281	0.017

Table S3: Recovery of each member across treatments normalized to *S. meliloti* plus individual treatment as represented in Figure 3A. Calculation used for normalization represented below.

Microbial Treatment	***Pseudomonas sp.* Ag47**	***Brevibacillus brevis* Ag35**	***Paenibacillus sp.* Ag47**	***Pantoea agglomerans* Ag15**
S. meliloti RM1021, Ag47	NA	NA	0	NA
S. meliloti RM1021, Ag15	NA	NA	NA	0
S. meliloti RM1021, Ag35	NA	0	NA	NA
S. meliloti RM1021, Ag54	0	NA	NA	NA
S. meliloti RM1021, Ag54, Ag35	0	0.1	NA	NA
S. meliloti RM1021, Ag35, Ag15	NA	-0.025	NA	0
S. meliloti RM1021, Ag35, Ag47	NA	0.4	0.164	NA
S. meliloti RM1021, Ag15, Ag47	NA	NA	-0.053	0
S. meliloti RM1021, Ag54, Ag47	0.833	NA	0.197	NA
S. meliloti RM1021, Ag54, Ag15	0	NA	NA	0
S. meliloti RM1021, Ag35, Ag15, Ag47	NA	0.503	-0.055	0
S. meliloti RM1021, Ag54, Ag47, Ag15	0.273	NA	0	0
S. meliloti RM1021, Ag54, Ag35, Ag47	0.105	-0.084	-0.478	NA
S. meliloti RM1021, Ag54, Ag15, Ag35	0.25	0.267	NA	0
S. meliloti RM1021, Ag54, Ag35, Ag47, Ag15	0.57	0.17	-0.355	0.017

$$\left(\frac{\text{Number of nodules where bacterium was recovered from treatment X}}{\text{Total number of nodules assayed from treatment X}}\right) - \left(\frac{\text{Number of nodules where bacterium was recovered from treatment w/ } \textit{S. meliloti} \text{ alone}}{\text{Total number of nodules assayed from treatment w/ } \textit{S. meliloti} \text{ alone}}\right)$$

Table S6. Summary table of interactions reported in Figure 3. Reported recovery (%) of each bacterium from treatments 4, 9, 12 and 15 (number of nodules that bacterium was recovered from divided by the total number of nodules assayed for that treatment). Average colony forming units (CFU) reported for each bacterium (total CFU divided by the total number of nodules assayed for that treatment). Fold change calculated for Paenibacillus sp. (the average CFU value of Paenibacillus sp. from the respective treatment divided by the average CFU for Paenibacillus sp. in Treatment 12). Fold change could not be reported for Pseudomonas sp. due to the zero in the baseline treatment 15. Baseline (purple text), positive (blue text), negative (red text) and neutral (black text) effects are highlighted as seen below.

(*S. meliloti* added to all treatments)		*Psuedomonas sp.*			*Paenibacillus sp.*			*B. brevis*	
Treatment	**Inoculum**	**Recovery (%)**	**Avg. CFU**	**Fold Change**	**Recovery (%)**	**Avg. CFU**	**Fold change**	**Recovery (%)**	**Avg. CFU**
15	*Pseudomonas sp.*	**0/15 (0%)**	**0.0**	**0.0/0.0**					
12	*Paenibacillus sp.*				**7/11 (63%)**	**280.9**	**280.9/280.9 (+1.0)**		
9	*Paenibacillus sp. and Pseudomonas sp.*	**10/12 (83%)**	**65.8**	**65.8/0.0 (Not Calculated)**	**10/12 (83%)**	**69.0**	**69.0/280.9 (-4.0)**		
4	*Paenibacillus sp., Pseudomonas sp. and B. brevis*	**2/19 (10%)**	**1.3**	**1.3/0.0 (Not Calculated)**	**3/19 (16%)**	**336.6**	**336.6/280.9 (+1.2)**	**6/19 (32%)**	**18.5**

Purple text = Baseline **Blue Text = Positive effect** **Red Text = Negative effect** **Black Text = Neutral effect**

Chapter 2 Supplemental Figures

Figure S1. 16S community profiling of the root nodule microbiome. 16S community profiling of young (Y), active (A) and senescent (S) root nodules from alfalfa plants grown at the Oxford Tract in Berkeley, CA(labeled Berkeley, Ca, right) and grown under lab conditions in soil collected from Hopland, CA(labeled Hopland, Ca, left). Roots were surface sterilized and root nodules removed and divided by phenotype for eDNA extraction.

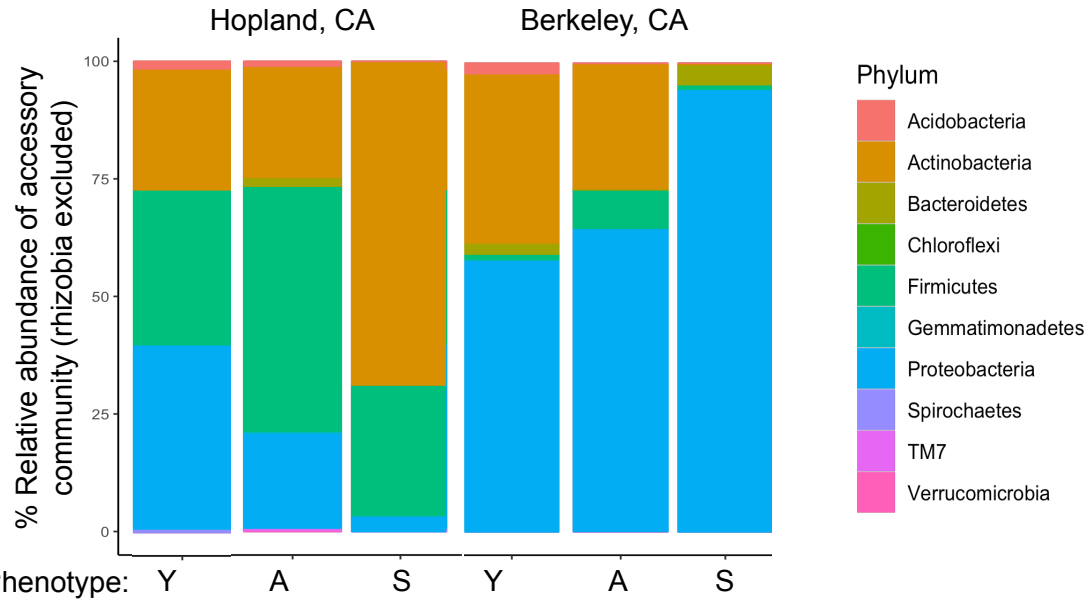

accessory community reads/total reads in %:	0.3	0.1	22.9	48.3	0.3	9.1

Figure S2. Plant height and nodule counts across microbial treatments reported in Figure 3. **(A)** Average plant heights of *Medicago sativa* after combinatorial inoculations (blue) with community members. Height recorded in centimeters. **(B)** Average number of root nodules per plant after combinatorial inoculations (blue) with community members. White boxes indicate corresponding member(s) were not added to treatment.

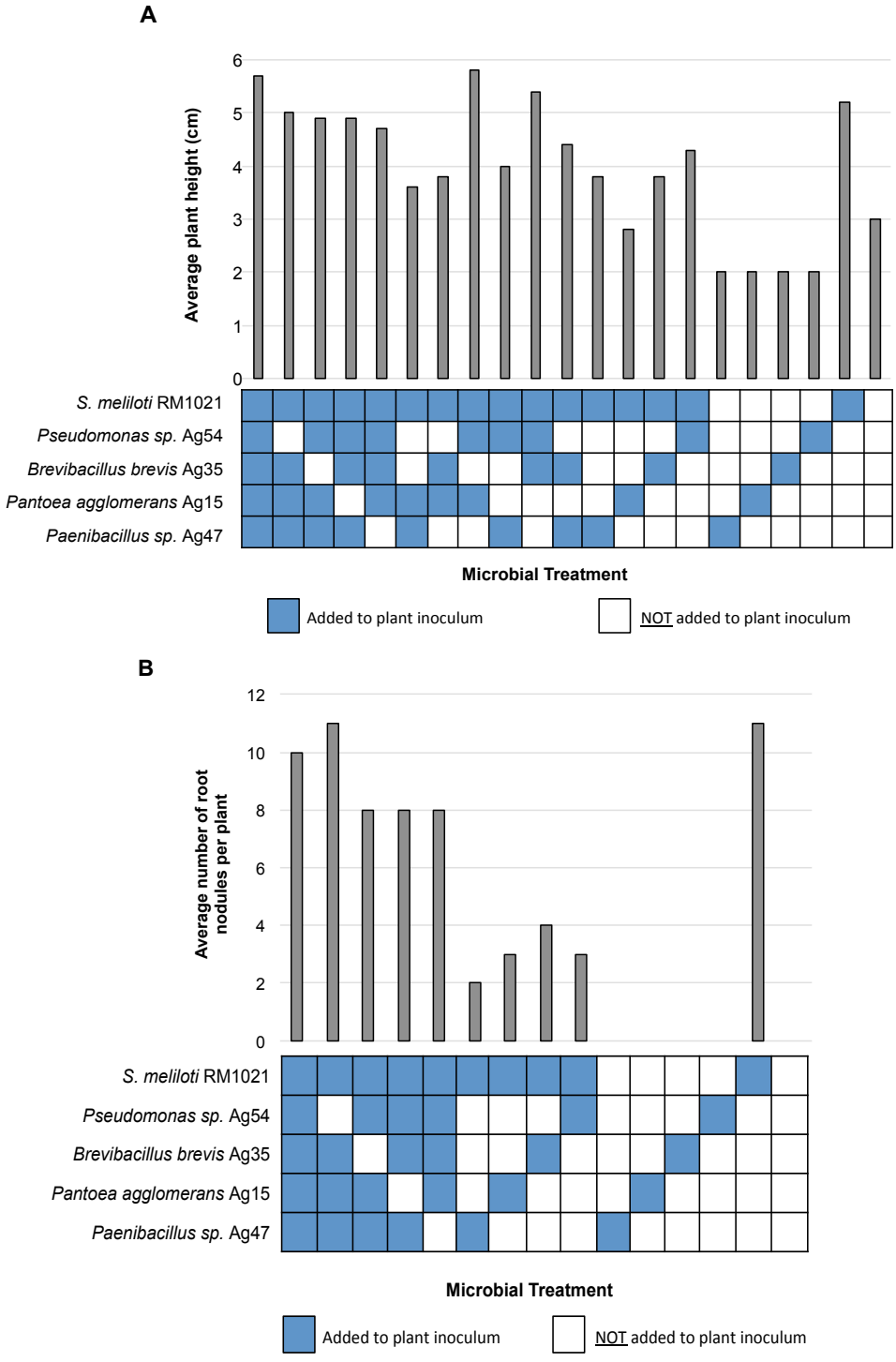

Figure S3. Venn analysis of all *in planta* community treatments. Venn diagrams represent all outcomes from each treatment reported in Figure 3. Numbers within circles represent number of nodules. “None” label represents no members recovered.

Treatment 1 – *Whole Community*

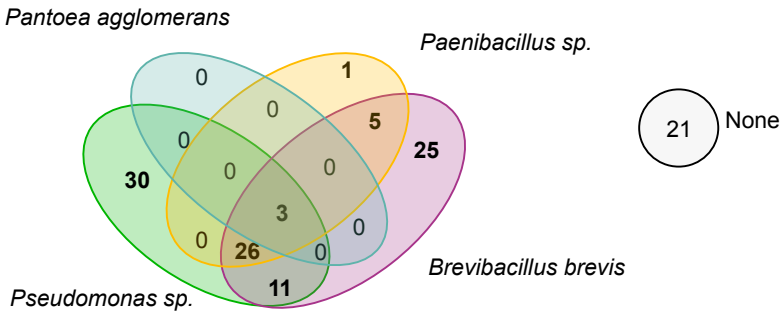

Treatment 2 – *B. brevis , P. agglomerans and Paenibacillus sp.*

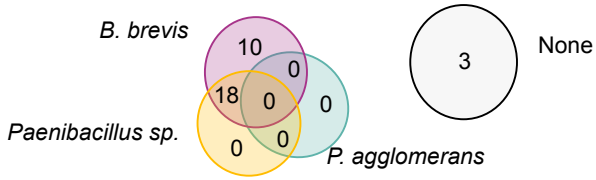

Treatment 3 – *Paenibacillus sp, Pseudomonas sp.* and *P. agglomerans*

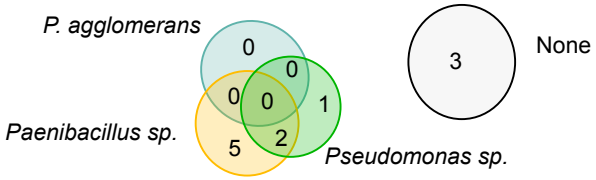

Treatment 4 – *Paenibacillus, Pseudomonas sp.* and *B. brevis*

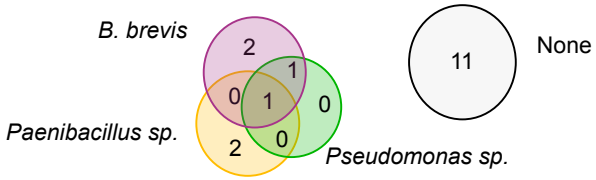

Treatment 5 – *P. agglomerans, Pseudomonas sp.* and *B. brevis*

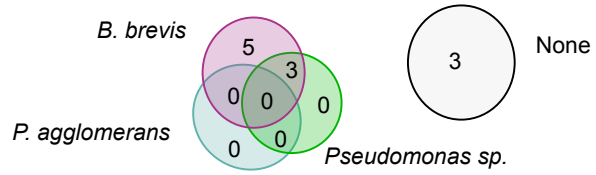

Treatment 6 – *Paenibacillus sp.* and *P. agglomerans*

Treatment 7 – *B. brevis* and *P. agglomerans*

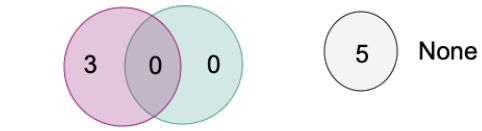

Treatment 8 – *P. agglomerans* and *Pseudomonas*

Treatment 9 – *Paenibacillus* and *Pseudomonas*

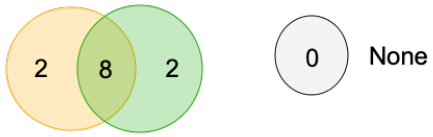

Treatment 10 – *B. brevis* and *Pseudomonas*

Treatment 11 – *Paenibacillus* and *B. brevis*

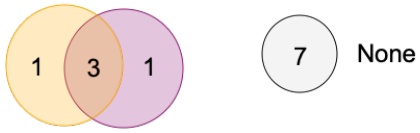

Treatment 12 – *Paenibacillus* alone

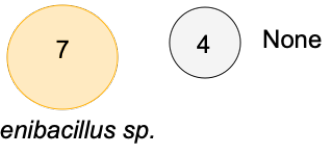

Treatment 13 – *P. agglomerans* alone

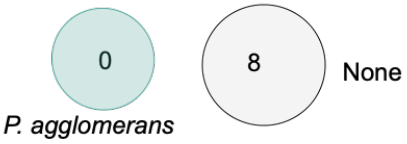

Treatment 14 – *B. brevis* alone

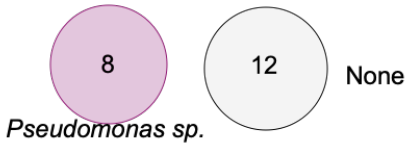

Treatment 15 – *Pseudomonas* alone

Figure S17: Fold change in recovered colony forming units (CFU) from all treatment conditions *in planta*. White boxes with a (+) indicate the bacterium was added to the treatment (x-axis, 1-15) and was recovered, but no fold change could be calculated because the bacterium inoculated with *S. meliloti* alone, was unrecoverable. White boxes with an NR indicate the bacterium was added to the inoculum but was not recovered from the root nodule. Empty white boxes indicate this bacterium was left out of the inoculum. Boxes with blue, grey or yellow, represent a fold change from the 1-member condition with yellow showing a strong positive fold change.

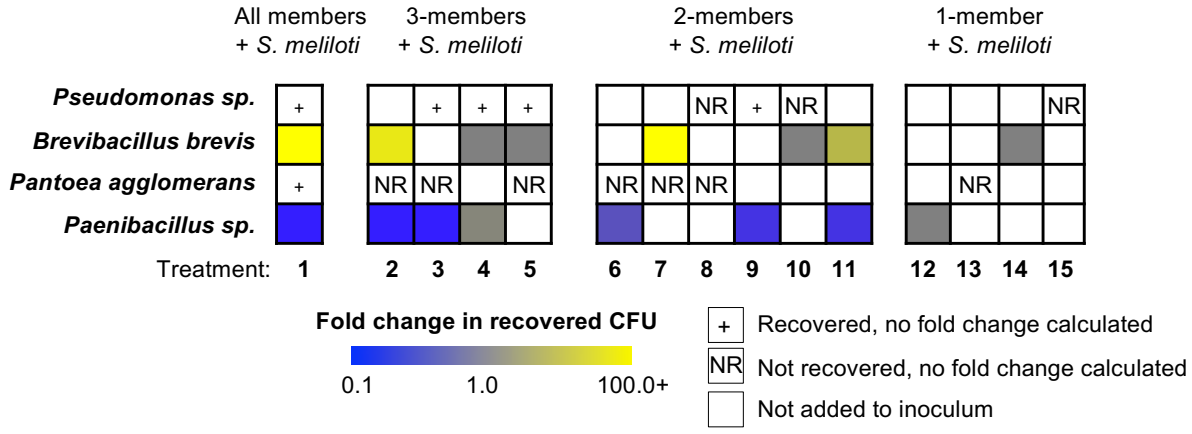

Chapter 3: Chemical analysis of the root nodule microbiome of Alfalfa

A portion of this chapter has been adapted from the following with permission:
Hansen, B.L., Pessotti, R.C., Fischer, M.S., Collins, A., El-Hifnawi, L., Liu, M.D. and Traxler, M.F. (2020) Cooperation, Competition, and Specialized Metabolism in a Simplified Root Nodule Microbiome. mBio. 11(40) e01917-20. doi: 0.1128/mBio.01917-20

3.1 Introduction

Drug discovery efforts have focused on optimizing the production and purification of specialized metabolites with a specific function of interest in mind, i.e. activity against a specific pathogen or an anti-cancer activity. Little work has been done to understand the role that specialized metabolites have in a microbial context. For example, does this microbe produce this antibiotic in nature and does it provide a competitive advantage to the microbe making it? How does this microbe and its antimicrobial repertoire impact microbiome structuring? To address questions like these, we require a model system containing microbes capable of making specialized metabolites.

Multiple reports have demonstrated that plant microbiomes contain members with strong potential as sources of novel specialized metabolites *in vitro* (33, 44, 45, 64, 88), however, relatively few studies have examined microbial specialized metabolism *in planta*(46, 89–101). Members of the genus *Pseudomonas* and the order *Rhizobiales* are notable exceptions, as genetic approaches have been used in these organisms to demonstrate the effect of specialized metabolites, which inhibited fungal pathogens(102, 103) or mediated microbe/host plant communication(49, 104), respectively. From a chemical perspective, our knowledge of specialized metabolism *in planta* is much more limited, with only a handful of reports demonstrating detection of antimicrobials *in planta*(105–108). Thus, while specialized metabolism appears to be widespread in plant microbiomes, many questions remain regarding when and where these molecules are produced *in planta*, and what their impact may be within these microbial communities.

Metabolomics, the study of metabolites within a given environment, has proved a useful approach for *in planta* root and nodule studies(43, 109, 110). The term metabolomics is deceiving because it is impossible to study the entire metabolome of a given sample at once due to the vast differences in chemical makeup of the metabolome, i.e. polarity, charge state, size, etc. However, focusing on a subset of the metabolome can lead to the identification of important ions within a given sample. Liquid chromatography tandem mass spectrometry (LC-MS/MS) is a powerful tool used for metabolomics studies that allows us to detect compounds present within a sample with high accuracy. This method paired with Matrix-assisted laser desorption/ionization imaging mass spectrometry (MALDI-IMS) can help address questions around detection and localization of a given compound within a sample. Using MALDI-IMS, we can generate a two-dimensional map of all ions within a sample.

In chapter 2, through using a simplified root nodule microbiome, we showed that *Brevibacillus brevis* Ag35 has antagonistic activity *in planta* and produces antagonistic molecules *in vitro*. We observed that *B. brevis* inhibited the growth of all other community members *in vitro* yet was isolated from root nodules where all members were present. This led us to ask, 1) what are the identities of these antagonistic molecules and are they made *in planta,* and 2) what is the spatial structure of this microbiome within the root nodule? In this chapter, we take a chemical approach

to identifying the antagonistic molecules produced by *B. brevis*, detect the compounds *in planta* and characterize the spatial structure of the root nodule community.

3.2 Results

3.2.1 Specialized metabolism *in planta*

To identify molecules/unique chemical features that could serve as signatures for each of the microbes in the community, we conducted a Venn analysis with the processed metabolomics data, as seen in Figure 4A. We identified chemical features that were not present in nodules containing only *S. meliloti*, but that were present in all three other treatments: 1) a single microbe grown *in vitro,* 2) the root nodule inoculated with this microbe, and 3) the root nodule inoculated with the whole community (Fig 4A, Supplemental Fig S4). The molecular features present in this intersection of treatments are unique to each microbe and also present in the root nodule inoculated with the whole community. To identify chemical features that were unique to each microbe compared to the other members of the community, we performed a second Venn analysis with the outputs of the first set of analyses (Fig 4A). We found zero unique features attributed to *Paenibacillus sp.* Ag47*,* four unique features for *P. agglomerans* Ag15*,* five unique features for *Pseudomonas sp.* Ag54 and 16 unique features for *B. brevis* Ag35 (Fig 4B). *S. meliloti* had the most unique features out of the five bacteria, with 37 features.

Since *B. brevis* Ag35 was the accessory community member that had the most unique features *in planta*, and it displayed the ability to inhibit growth of all other members of the community (Fig. 3C), we concluded that *B. brevis* Ag35 might be a promising candidate for further exploration of specialized metabolism within the root nodule. We started with the set of 16 unique chemical features from the second analysis for this microbe and compared it to features observed from two root nodule communities that did not include *B. brevis* Ag35. Specifically, the two communities used for this comparison were the entire community, except *B. brevis* Ag35, and a community consisting of *S. meliloti* RM1021, *P. agglomerans* Ag15, and *Paenibacillus sp.* Ag47. This analysis left 13 features that were unique to *B. brevis* Ag35 (Fig 4C& Supplemental Table S4).

3.2.2 MALDI-IMS of the simplified community root nodule

Since we identified several microbe-specific chemical features, we sought to leverage these data to examine the distributions of species-specific chemical features/ions within nodule tissues. Detection of microbe-specific features *in planta* might allow these features to be aligned with key plant physiological processes, and/or might shed light on the distribution of each microbe. We employed high-resolution matrix-assisted laser desorption/ionization imaging mass spectrometry (MALDI-IMS), which provides a two-dimensional map of molecular features in a sample. We applied this method to the surface of a 20-micron thick slice from an active root nodule that was inoculated with the whole community, with a pixel size of 10 μm (Fig. 5, Supplemental Fig. S16). We observed a feature with a *m/z* of 616.2 that was localized in an area proximal to the site of stem attachment. This ion (*m/z* 616.2) had an exact mass and fragmentation pattern (observed by LC-MS/MS) that matched published data for the identification of heme B(111) and a protoporphyrin standard (Supplemental Fig. S5 & Table S5). Thus, we ascribe this feature to heme B associated with leghemoglobin produced by *M. sativa* within the nodule region where active nitrogen fixation would be expected.

Based on the analysis in Figure 4, we next checked for features that were diagnostic for each of the microbial members of the system. A feature associated exclusively with *S. meliloti* RM1021,

m/z 536.4, showed strong co-localization with the heme ion noted above. This co-localization is significant and expected because it is consistent with the presence of *S. meliloti* RM1021 in the region of nitrogen fixation. We also observed that a feature unique to *B. brevis* Ag35, *m/z* 617.4, was detected in the central area of the nodule, with little or no overlap with the *S. meliloti* RM1021 feature *m/z* 536.4. Finally, we observed a feature with *m/z* of 763.0, which was uniquely associated with the entire community, meaning this feature was only detected in nodules that were inoculated with all members of our simplified nodule microbiome. This feature was localized in the distal part of the root nodule, in an area distinct from the features associated with *S. meliloti* RM1021 and *B. brevis* Ag35. Taken together, these data demonstrate that features associated with at least two members of this simplified community, and possibly more, are detectable in different regions of the nodule, indicating that these microbes may reside in distinct locations *in situ*.

3.2.3 Identification of *Brevibacillus brevis* Ag35 secondary metabolites

Because we were able to detect *B. brevis* Ag35 features *in planta* using both LC/MS and MALDI-IMS methods, we focused on identifying some of the features observed in the metabolomics data (Figure 4). Out of the 13 ions specific to *B. brevis* Ag35 found in the root nodule extracts, we identified *m/z* 1270.66, as the $[M+H]^+$ adduct of Tyrocidine A (**1**), a non-ribosomal peptide (NRP). We verified this identification by comparing its exact mass, retention time and fragmentation pattern to an authentic standard of Tyrocidine (Fig. 6B, Supplemental Fig. S6 & Table S5). We also found *m/z* 635.83, representing the $[M+2H]^{2+}$ ion of Tyrocidine A (**1**). Further analysis of extracts from *B. brevis* Ag35 grown *in vitro* revealed that this strain also produced Tyrocidine B (**2**) indicated in Figure 6A, Supplemental Fig. S7 & Table S5.

Among the features associated with *B. brevis* Ag35 *in planta*, we observed another ion, *m/z* 1033.08 (Supplemental Table S4), that had an MS1 pattern (Supplemental Fig S8) indicative of a double charged species and a fragmentation pattern similar to that of the gramicidin-family compounds (Supplemental Fig. S9). The gramicidins are antibiotic NRPs known to be produced by *B. brevis* ATCC 8185(112). Further analysis of *m/z* 1033.08 revealed it to be the $[M+H+Na]^{2+}$ species of a novel molecule we have termed Britacidin A (**3**). Beyond this, we note that we also detected the $[M+2H]^{2+}$ (*m/z* 1022.0960), $[M+H+Na]^{2+}$ (*m/z* 1033.0848), and $[M+2Na]^{2+}$ (*m/z* 1044.0746) adducts of this compound in extracts from root nodules inoculated with the community containing *Brevibacillus brevis* Ag35 (dominant isotope from $[M+2H]^{2+}$ (*m/z* 1022.60) shown in Figure 6C, Supplemental Fig S8&S10, Table S5). Britacidin A (**3**) has an exact mass of 2042.1757 and shares structural similarities with Gramicidin A (compared in Fig. 7A). Through a combination of fragmentation analyses and ^{13}C labeling experiments, we determined that Britacidin A differs from Gramicidin A in three key ways: 1) at the first position, the dominant amino acid is isoleucine rather than valine (Figure 6B & 7A, Supplemental Fig. S15), 2) britacidin contains additional valine and alanine residues incorporated at positions 7 and 8 (Figure 6A & 7A, Supplemental Fig. S11), and 3) at position 11, britacidin contains tyrosine as the dominant amino acid, a position that is invariably tryptophan in gramicidins (Figure 6A & 7A, Supplemental Fig. S11). We identified two other analogs, termed Britacidin B (**4**) and C (**5**), also made by *B. brevis in vitro* (Figure 6A, Supplemental Fig. S12&13). We identified the minimum inhibitory concentration (MIC) of a Britacidins mixture to be 81 μg/ml using a liquid-dilution method against *Bacillus subtilis* 168 (Supplemental Methods). Taken together, these data indicate that *B. brevis* produced a known antimicrobial (Tyrocidine A), and a novel gramicidin-family antimicrobial (Britacidin A) *in planta*.

3.2.4 The Britacidin biosynthetic gene cluster

To identify a putative gene cluster responsible for production of the britacidins, we sequenced the genome of *B. brevis* Ag35 [NCBI Accession: JAAKZO000000000] and annotated the biosynthetic gene clusters using AntiSMASH 5.0(113). We identified the presence of eleven putative biosynthetic gene clusters, including one that matched a typical tyrocidine gene cluster with 81% similarity, and a gramicidin-like gene cluster with 91% similarity. We focused on the gramicidin-like gene cluster, which we propose to be responsible for britacidin production, thus we term them the *bri* genes (Figure 7A&B). Within NRPS enzymes, the ten amino acid residues that surround the binding pocket within the adenylation (A) or AMP-binding domains determine which amino acid is added to the growing peptide. There are several key differences between the canonical gramicidin gene cluster encoded by *B. brevis* ATCC 8182, and the putative britacidin gene cluster encoded by *B. brevis* Ag35. First, two additional AMP-binding domains were found in *briB,* the second predicted NRPS gene in the cluster (Figure 7B). These additional A domains are predicted to incorporate the extra alanine and valine residues (Figure 7B&C) at positions 7 and 8 (Figure 7A). These additional domains and predictions correlate directly with the structure determined for the britacidins described in Figure 6A and Figure 7A. The residues that define the binding pocket in A domains can be condensed into a sequence, known as the Stachelhaus sequence, which can be used to predict the identity of amino acids incorporated by NRPS enzymes and compare A domains(114). Another key difference between the canonical gramicidin gene cluster and the putative britacidin gene cluster lies in the Stachelhaus sequence of the A domain that determines the amino acid found in position eleven of britacidin, which we propose to incorporate a tyrosine residue based on structural elucidation of Britacidin A-C. In the gramicidins, the corresponding residue is almost always a tryptophan. Accordingly, we note that the Stachelhaus sequence of the corresponding A domain in the britacidin cluster varies significantly from the Stachelhaus sequence of the corresponding position in the canonical gramicidin cluster (Figure 7C, Supplemental Fig. S14). For position 13, the amino acid varies in both the Gramicidins and Britacidins and the Stachelhaus sequence for this position is nearly identical across the two (Figure 7A&C, Supplemental Fig, S14). Overall, the novel structural features of the britacidins are accounted for by the unique variations observed in the *bri* gene cluster encoded in the genome of *B. brevis* Ag35.

3.3 Discussion

Microbes have been known to produce specialized metabolites, like antibiotics, *in vitro*, however, knowledge of production within the context of the natural environment is limited. An untargeted metabolomics strategy, combined with a subtractive analysis pipeline, enabled us to attribute different chemical features to the plant and individual microbes within the simplified nodule community both *in vitro* and *in planta*. In addition to highlighting the britacidins and tyrocidines, this analysis yielded diagnostic molecules for *B. brevis*, *S. meliloti*, and *M. sativa*. We next used high-resolution, sub-atmospheric MALDI mass spectrometry imaging to assess the spatial distributions of these diagnostic molecules within cross-sectioned nodules. Velickovic and co-workers observed metabolic asymmetry in the root nodule highlighting the spatial complexity that can exist within this system(110). Our imaging mass spectrometry analysis revealed a strong spatial correlation between heme B, likely associated with the leghemoglobin of the nodule, and a chemical feature associated with *S. meliloti*. The region of high overlap between these signals likely defines the area where N-fixation occurs. We also observed that a chemical feature

associated exclusively with *B. brevis* was found in a region distinct from the areas defined by heme and *S. meliloti* signals. We interpret this to mean that *B. brevis* likely inhabits areas of the nodule outside of the region of active N fixation. Beyond this, a chemical feature which was strictly associated with nodules inoculated with the entire four-member accessory community was observed in yet another region of the nodule distinct from the areas with signals diagnostic of *B. brevis* or *S. meliloti*. Together, these results indicate that the members of the nodule community are likely spatially segregated within the nodule. Such segregation may arise from competitive exclusion within this community(115).

In total, the findings presented here indicate that root nodules, dedicated organs for the critical activity of N fixation, also host a microbiome with members that actively produce antimicrobials. We speculate that production of antimicrobials in the context of the nodule might influence the content and ultimately the function of the resident microbiome. Moreover, antimicrobial biosynthesis could also provide protection from pathogens that might infect these organs, thus ensuring that the critical activity of N-fixation is preserved. The simplified root nodule community that we developed here is a tractable system for directly exploring these potential roles for specialized metabolites. Beyond this, the nodule microbiome community may be ideal for pursuing key outstanding questions in the field of microbiome science, such as mechanistic exploration of spatial structuring, or evaluating cooperation and competition in the context of plant microbiomes.

Recent studies of interactions within synthetic communities based on plant microbiomes have found widespread inhibitory interactions and led to discovery of novel antimicrobial compounds. For example, the THOR model rhizosphere microbiome, presented by Lozano and co-workers, 2019, was found to contain *Pseudomonas koreensis*, the producer of koreenceines A-C(45). These molecules had inhibitory activity against another member, *Flavobacterium johnsoniae*. In another example, in the phyllosphere model presented by Helfrich and co-workers, binary interaction networks were created and bioactivity-guided fractionation led to the discovery of multiple novel molecules produced by *Brevibacillus sp*. Leaf182, including marthiapeptide A and phosphobrevin(44). Similarly, in our root nodule system, inhibitory interactions were common. *B. brevis* was particularly notable, as it produced strong antibiotic activity and was capable of inhibiting the growth of every other member. We found that a component of the antibiotic activity produced by *B. brevis* was attributable to a set of novel gramicidin-family metabolites we term the britacidins. Structurally, the britacidins differ from typical gramicidins in that they 1) feature an extended peptide backbone including additional alanine and valine residues, and 2) they frequently contain tyrosine residues at positions eleven and thirteen, which are usually tryptophan residues in typical gramicidins. These structural modifications coincided with a putative gene cluster found in the *B. brevis* genome with extremely high fidelity. This is notable from a biosynthetic standpoint, as the gramicidin NRPS enzymes have recently been the focus of interest from structural, catalytic, and bioengineering perspectives(116, 117). Thus, the britacidin gene cluster may have value as a natural source for alternative functionality within a well-understood enzymatic system.

Brevibacilli have been isolated in many studies aiming to identify plant-growth-promoting-rhizobacteria and are well-known producers of a range of antimicrobial compounds including the gramicidins and cyclic peptides of the tyrocidine family. Thus, our findings, together with the findings of Helfrich *et al*.(44) reinforce the idea that *B. brevis* may be a widespread member of plant microbiomes with a strong capacity for specialized metabolism. In keeping with this notion,

the *B. brevis* strain from this nodule community produced tyrocidine A and B, in addition to the britacidins. We also examined specialized metabolism *in planta* by using high-resolution metabolomics to characterize extracts from root nodules inoculated with our simplified nodule community. This led to the key finding that both the britacidins and tyrocidines were detectable in these extracts, indicating that *B. brevis* specialized metabolism is active *in planta*.

3.4 Materials and Methods

3.4.1 *In vitro* bacterial growth on root nodule medium and chemical extraction

Each bacterium was grown on Lennox LB-agar at 30°C overnight and single colonies were transferred to 5 mL Lennox LB liquid cultures. Cultures were shaken at 200 rpm overnight at 30°C, cells were pelleted, washed with ddH_2O and the OD_{600} was adjusted to 0.5. All bacteria were spotted at a volume of 1.5 μL in quadruplicate on Root nodule medium (5g/L malic acid, 1g/L casamino acids, 0.2g/L NaCl, 0.2g/L K_2HPO_4, 0.2g/L $MgSO_4$-7H_2O, 1mg/L H_3BO_3, 1mg/L $ZnSO_4$-7H2O, 0.5mg/L $CuSO_4$-5H_2O, 0.5mg/L $MnCl_2$-4H_2O, 1mg/L NaMoO4-2H_2O, 0.1g/L $FeCl_3$-6H_2O, and 18g/L agar, pH 7.5). After three days, four plugs were removed from the plate and extracted in MeOH-washed 1.5 mL eppendorf tubes with 500 μL MeOH, sonicated for five minutes and incubated for 12 hours at room temperature. MeOH was removed and transferred to clean MeOH-washed eppendorf tubes. Extracts were dried down using a speedvac at 45°C and stored at -20°C until samples were ready to be processed.

3.4.2 LC/HRMS analysis

Samples were re-suspended in a 150 μL of LC/MS grade MeOH/100nM reserpine solution, sonicated for 10 minutes, vortexed and spun down for 10 minutes at 15,000 rpm to ensure no particulate was in the sample. 100 μL was transferred into an insert and 50 μL transferred to a pooled quality control (QC) mix comprised of all samples. Using a random number generator, samples were analyzed in a random order. Samples were analyzed by a Ultra-High Pressure Liquid Chromatography (UHPLC) system (Dionex Ultimate 3000, ThermoFisher, USA) coupled to a high resolution mass spectrometer (HRMS, Thermo Q-Exactive Quadrupole-Orbitrap, ThermoFisher, USA) using a Heated Electrospray ionization (HESI) source, using a C18 column (50 mm x 2.1 mm, 2.2 μm, Thermo Scientific AcclaimTM RSLC). The UHPLC method was as follows: 0-1 minute 10% ACN + 0.1% FA, a gradient from 1-11 minutes of 10% to 98% ACN + 0.1% FA, 11-14.5 minutes of 98% ACN + 0.1% FA and re-equilibration of the column back into 10% ACN + 0.1% FA from 14.5-18 minutes, injection volume of 5 μL, flow rate of 0.4 mL/min and column oven at 35 °C. The full MS1 scan was performed in positive mode, resolution of 35,000 full width at half-maximum (FWHM), automatic gain control (AGC) target of 1 x 10e6 ions and a maximum ion injection time (IT) of 100 ms, mass range from m/z 200-2000. MS/MS analysis was acquired using a data-dependent Top5 method at a resolution of 17,500 FWHM, AGC target of 1 x 10e5 ions and maximum ion IT of 50 ms, using an isolation window of 3 *m/z* and normalized collision energy (NCE) of 20, 30 and 45. Cone spray voltage was 3.5kV. Data was processed using MS-DIAL and analyzed using R v3.6.1, the data.table R package(118) and Venn diagrams were made using Adobe Illustrator v23.1.1.

3.4.3 Sample preparation and acquisition of MALDI-IMS

Fresh roots with root nodules were embedded in gelatin as described in Gemperline *et al*, and sliced at 20 μm using a cryostome (Leica CM3050 S) at -25°C (111). Slices were transferred to an

indium-tin oxide (ITO) coated microscope slide and stored at -20°C until samples were ready to be processed. Samples were thawed at room temperature inside a desiccator under vacuum (0.6 MPa) for 30-45 min. Micrographs of the root nodule slices were acquired using a ZEISS microscope (Zeiss AxioZoom v.16 equipped with Axiocam 506 color camera) and Super-DHB MALDI matrix (Sigma-Aldrich) was deposited on the top of the samples using a sublimation method described by Pessotti et al 2019 to achieve a spatial resolution of 10 μm(106). MALDI-IMS was performed in positive mode using a SubAP/MALDI(ng) source (MassTech, Columbia, MD) coupled to a Thermo Q-Exactive HRMS. Full MS1 scans were acquired in positive mode, resolution of 35,000 full width at half-maximum (FWHM), at mass range of *m/z* 100-2000, AGC target of 1 x 10^6 ions and a maximum IT of 400 ms. The pixel size was 10 μm at a laser velocity of 1.5 mm/min and laser energy of 50% at 1 kHz repetition rate. Imaging processing and analysis were performed using Datacube Explorer v2.3(119), MSiReader v1.01(120), and ImageJ v1.52a(121).

3.4.4 gDNA extraction, sequencing, and assembly of *Brevibacillus brevis* Ag35 genome

Brevibacillus brevis Ag35 was grown at 30C, shaking at 200 rpm in 20 ml of Lennox LB for 24 hours. Cells were pelleted at 4,000 rpm for 10 minutes at 4C. Protocol was adapted from Pacific Biosciences recommended gDNA cleanup with modifications. Pellet was washed with 10mM Tris-HCl,1mM EDTA, pH 8.0. Cells were re-suspended in 740ul 10mM Tris-HCl, 1mM EDTA, pH 8.0, treated with 2mg/ml lysozyme and incubated for 30 minutes. 40ul of 10% (w/v) SDS and 10ul proteinase K was added and the solution was incubated at 55C for 60 minutes. After solution cleared, 100ul 5M NaCl was added and the solution was incubated at 65C for 10 minutes. Solution was then cooled on ice, and then 1:1 volume chloroform:isoamyl alcohol (24:1) was added. Solution was inverted 20 times and phases were separated by centrifugation at 5000 rpm for 10 minutes. Top phase was transferred to a new tube and 1:1 volume of phenol:chloroform:isoamyl alcohol (25:24:1), pH 8.0 was then added. Solution was inverted and phases separated by centrifugation at 500 rpm for 10 minutes. Top phase was transferred and 1:1 volume chloroform:isoamyl alcohol (24:1) step with centrifugation was repeated. Top phase was transferred and gDNA was fished out using a clean p1000 pipette tip and transferred to a fresh tube. gDNA was washed with ice cold isopropanol followed by ice cold ethanol. Genomic DNA was then resuspended in 10mM Tris-HCl, 1mM EDTA, pH 8.0, treated with RNase at 37C for 15 minutes followed by the addition of 1:10 volume 3M sodium acetate. Two volumes of cold ethanol was then added to precipitate the DNA and then was fished out using a clean p1000 pipette tip and transferred to a fresh tube. DNA was washed with 75% ethanol and air dried. DNA was sequenced using PacBIO technologies. Sequencing data was partitioned using seqtk followed by genome assembly with Flye at 222x coverage. Genome was annotated using AntiSMASH 5.0.

3.4.5 Purification and antimicrobial activity of Britacidins

B. brevis Ag35 was grown on ISP2 agar for 48 hours, extracted 2:1 with EtAc. Size exclusion chromatography was performed in a 1.5 cm diameter glass column using Sephadex LH-20 resin swelled in methanol for 3 hours at room temperature (18g of resin 72 mL of methanol). The column was packed under gravity for a final bed height of 41 cm. The column was equilibrated with 2 CV of methanol. The dry sample (27.5 mg) was re-suspended in 1.4 mL, sonicated and then centrifuged for 2 minutes at 10,000 x g and the supernatant was loaded onto the column. Eluents were collected under gravity flow. The first 32 mL were discarded. The next 12 mL were collected and run on LC/HRMS to confirm purity.

3.4.6 Structural Elucidation of Britacidins

The unknown feature *m/z* 1033.0829 detected in the root nodules was also detected in *B. brevis* cultures. Three other features were observed in the same MS1 spectrum: *m/z* 1022.0960, 1033.0848, 1044.0746, 2043.1830 and 2065.1664. The isotopic pattern and MS2 spectra suggested that these five features are different adducts of the same compound, specifically: *m/z* 1022.0960= $[M+2H]^{2+}$, *m/z* 1033.0848= $[M+H+Na]^{2+}$, *m/z* 1044.0746= $[M+2Na]^{2+}$, *m/z* 2043.1830 = $[M+H]^{+}$ and *m/z* 2065.1664= $[M+Na]^{+}$. Database searches did not provide any hits with known molecules. The observed fragmentation pattern proved to be very similar to the fragmentation of the analytical standard of Gramicidin A obtained from *B. brevis* (Sigma-Aldrich) (Supplemental Fig S9). Therefore, it was hypothesized that this unknown feature is a new analog of the Gramicidin family.

In order to investigate the structure of this potentially novel compound, we used a low normalized collision energy (NCE 15) that allowed us to see the amino acids losses of the $[M+2H]^{2+}$ and $[M+H]^{+}$ adducts. The largest fragment detected in common between Gramicidin A and the unknown feature was *m/z* 959.5511, that corresponds to the Gramicidin A protonated Y_6 product ion ($C_{53}H_{71}N_{10}O_7^{+}$, with a measured error of 0.94 ppm, Supplemental Fig S9 &11), which suggests that this compound and Gramicidin A differ structurally from positions 1-13 (Figure 7A & Supplemental Fig. S9). The *b* product ion series are of higher abundance when compared to the *Y* series and therefore was chosen to follow the successive amino acid losses to elucidate the unknown molecule. Supplemental Table S11 shows all the detected amino acids losses and summarizes the suggested chemical formula and ppm error of each predicted ion of both *b* and *y* series.

The fragmentation pattern revealed that when compared to Gramicidin A the unknown compound, termed Britacidin A (Figure 7A), has two additional alanine and valine residues at positions 7 and 8, and a tyrosine at position 11 instead of a tryptophan. The common substitution in the Gramicidin family from valine to isoleucine at the first amino acid position(112) was observed: fragments *m/z* 114.09 and 142.08 corresponds respectively to the a_1 and x_1 product ions that results from the fragmentation between the glycine residue at position 2 and isoleucine residue at position 2 (Fig 7A). Because isoleucine and leucine are the same molecular weight, we performed ^{13}C-isoleucine and ^{13}C-leucine feeding experiments (Supplemental Methods) to determine the identity of the amino acid at position 1 to be isoleucine (Supplemental Fig. S15).

Other Britacidin analogs were observed, but only two of them were abundant enough to allow structural elucidation using fragmentation patterns. These analogs were named Britacidin B and C (Figure 6A, Table S12&13).

3.4.6 ^{13}C-isoleucine and ^{13}C-leucine feeding experiments and LC/HRMS

To determine the identity of the amino acid at position 1 on Britacidin A-C, we grew *B. brevis* Ag35 in minimal medium supplemented with either 150 mg/L ^{13}C-isoleucine (Cambridge Isotope Laboratories, Inc) or ^{13}C-leucine (Cambridge Isotope Laboratories, Inc). The minimal medium contained: 12.8 g/L Na2HPO4, 3.0 g/L KH2PO4, 0.5 g/L NaCl, 1.0 g/L NH4Cl, 20 mL/L of 20% glucose solution, 2 mL/L of 1M MgSO4 solution, 0.1 mL/L of 1M CaCl2 solution, 10 mL/L of RPMI 1640 B vitamins mixture (Sigma) and 150 mg/L of each of the 20 amino acids (control) or without isoleucine (supplemented with 1mg/mL ^{13}C-labelled isoleucine) or without leucine (supplemented with 1mg/mL ^{13}C-labelled leucine). 8 mL liquid cultures were adjusted to an O.D.600 of 0.05 from *B. brevis* Ag35 starter cultures in control medium and incubated at 30 oC

shaking at 200 rpm for 48 hours. Cultures were extracted with 1:1 EtAc. The EtAc fraction was dried down and re-suspended in 80 µL MeOH, which was then transferred to a glass insert. Samples were analyzed by a Ultra-High Pressure Liquid Chromatography (UHPLC) system (Dionex Ultimate 3000, ThermoFisher, USA) coupled to a high resolution mass spectrometer (HRMS, Thermo Q-Exactive Quadrupole-Orbitrap, ThermoFisher, USA) using a Heated Electrospray ionization (HESI) source, using a C18 column (50 mm x 2.1 mm, 2.2 µm, Thermo Scientific AcclaimTM RSLC). The UHPLC method was as follows: 0-1 minute 10% ACN + 0.1% FA, a gradient from 1-11 minutes of 10% to 98% ACN + 0.1% FA, 11-14.5 minutes of 98% ACN + 0.1% FA and re-equilibration of the column back into 10% ACN + 0.1% FA from 14.5-18 minutes, injection volume of 5 µL, flow rate of 0.4 mL/min and column oven at 35 °C. The full MS1 scan was performed in positive mode, resolution of 35,000 full width at half-maximum (FWHM), automatic gain control (AGC) target of 1 x 10e6 ions and a maximum ion injection time (IT) of 100 ms, mass range from m/z 200-2000. MS/MS analysis was acquired using a data-dependent Top5 method at a resolution of 17,500 FWHM, AGC target of 1 x 10e5 ions and maximum ion IT of 50 ms, using an isolation window of 3 *m/z* and normalized collision energy (NCE) of 20, 30 and 45. Cone spray voltage was 3.5kV.

3.4.7 Minimum inhibitory Concentration of Britacidins mixture

Minimum inhibitory concentrations of Britacidins and Gramicidins were measured against the gram-positive bacterium, *Bacillus subtilis* 168 using a broth micro-dilution method (Wang F, Qin L, Pace CJ, Wong P, Malonis R, Gao J. 2012. ChemBioChem 51–55). Specifically, *B. subtilis* was grown on LB agar overnight at 30 oC; a single colony was transferred to a 3 ml liquid LB culture for overnight incubation shaking at 30 oC. 100 µL from the culture was transferred into 3 ml of LB and incubated for 2 hours at 30 degrees oC. OD600 was taken and adjusted to 0.1 and 100 µL were transferred/added to the micro-wells of the 96-well plate containing 100 µL of 2-fold serial dilutions of the antibiotic (dissolved in DMSO) in LB. DMSO starting concentration was 3%. Range tested was 80 µM to 0.3 µM calculated based on Britacidin A. An initial plate reading was taken at 590 nm, plate was incubated at 30 oC and 16 hours later, a second reading was taken. The MIC was determined based on the absence of growth in triplicate. Because <1 mg of Britacidins were purified for the assay, the final calculated MIC value could be lower due to limitations in the sensitivity of our weigh scale.

Chapter 3 Figures

Figure 4. Number of molecular features associated with the simplified nodule community *in vitro* and *in planta*. Molecular features identified via LC/MS from chemical extracts that were prepared from three independent treatments of each microbe: alone on agar plates (*in vitro*), inoculated onto *M. sativa* plants individually with *S. meliloti*, or inoculated onto *M. sativa* plants with all other members of the simplified nodule community, plus an additional control treatment of *M. sativa* plants inoculated solely with *S. meliloti*. **(A)** Depicts our analysis approach using nested Venn Diagrams to identify features that are unique to each microbe, and then we focused on unique features associated with *B. brevis* both *in planta* and *in vitro* when compared to all other community members. **(B)** Number of features that are unique to each microbe. **(C)** Number of features that are unique to *B. brevis* compared with the number of features identified in two different simplified communities lacking *B. brevis in planta*. The 13 features that are unique to *B. brevis in vitro* and *in planta* are highlighted as features of interest and detailed in Table S4.

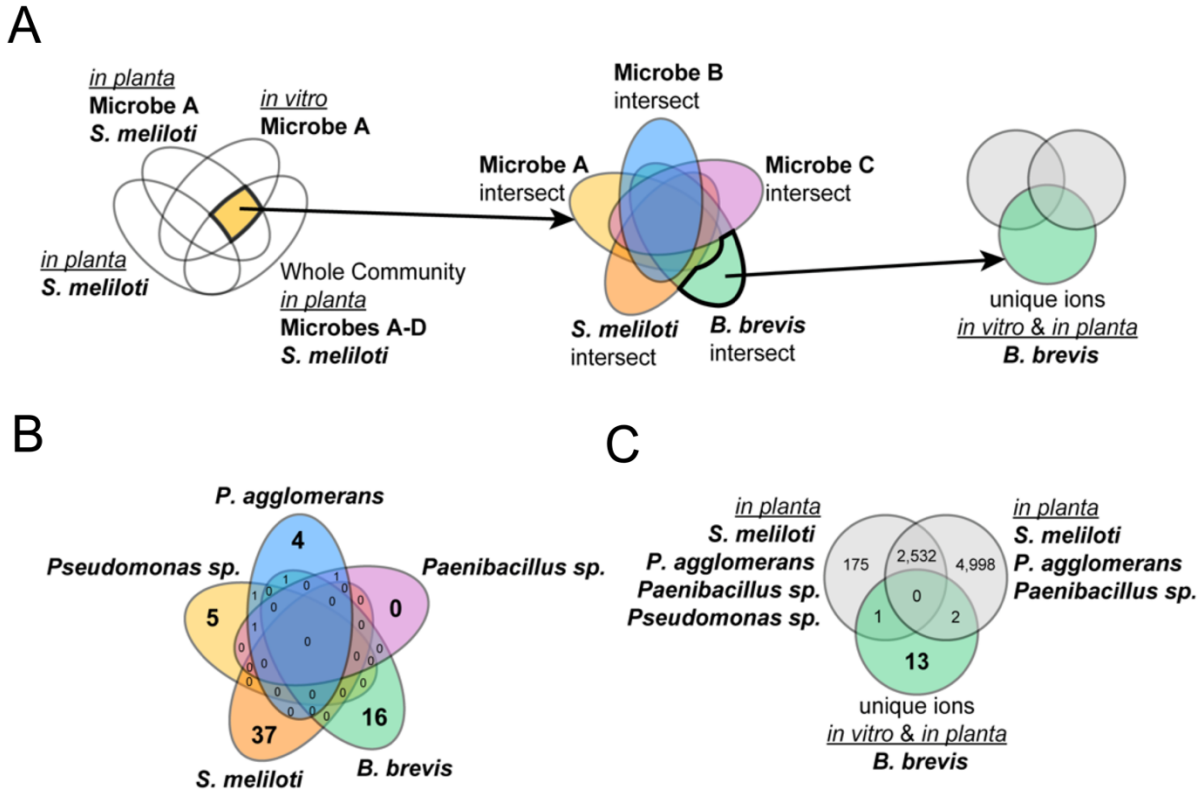

Figure 5. MALDI images of the simplified community root nodule. Brightfield image of a 20 μm thick simplified community root nodule embedded in gelatin. The ion for Heme B, *m/z* 616.2 (magenta), and an unidentified feature, *m/z* 536.4 (cyan), are unique to *S. meliloti* and co-localize. In contrast, the feature *m/z* 617.4 is associated with *B. brevis*, and an unidentified feature associated with the community, *m/z 763.0* are spatially distinct (Overlay).

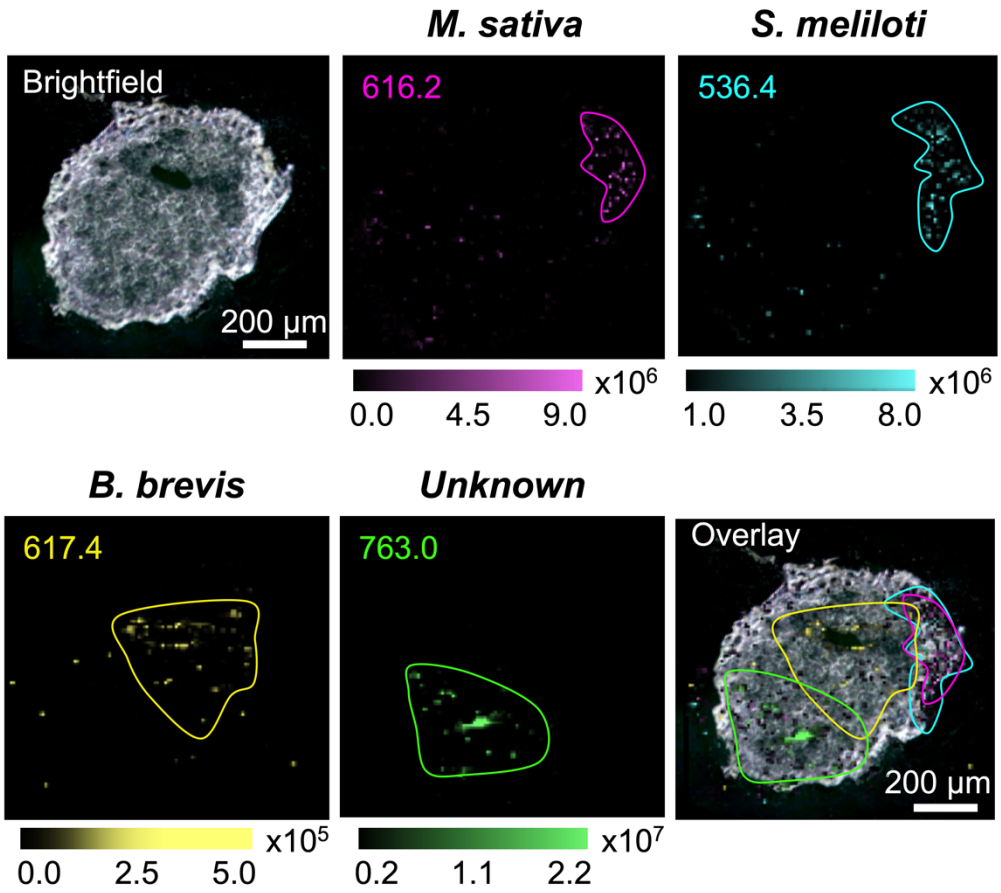

Figure 6: Tyrocidine A and Britacidin A are detected *in planta*. A) Tyrocidine A (1) and B (2) and Britacidin A (3), B (4) and C (5) are produced by *B. brevis*. (*) denotes that this molecule was detected *in planta* (Tyrocidine A and Britacidin A). **B)** Extracted ion chromatogram of the $[M+H]^+$ Tyrocidine A, *m/z* 1270.66, from: Tyrocidine standard, *B. brevis* grown *in vitro* on root nodule medium, methanol extracts of community root nodules and methanol extracts of *S. meliloti* only root nodules. **C)** Extracted ion chromatogram of the dominant isotope of the $[M+2H]^{2+}$ species of Britacidin A, *m/z* 1022.60, from: *B. brevis* grown *in vitro* on root nodule medium, methanol extracts of community root nodules and methanol extracts of *S. meliloti* only root nodules.

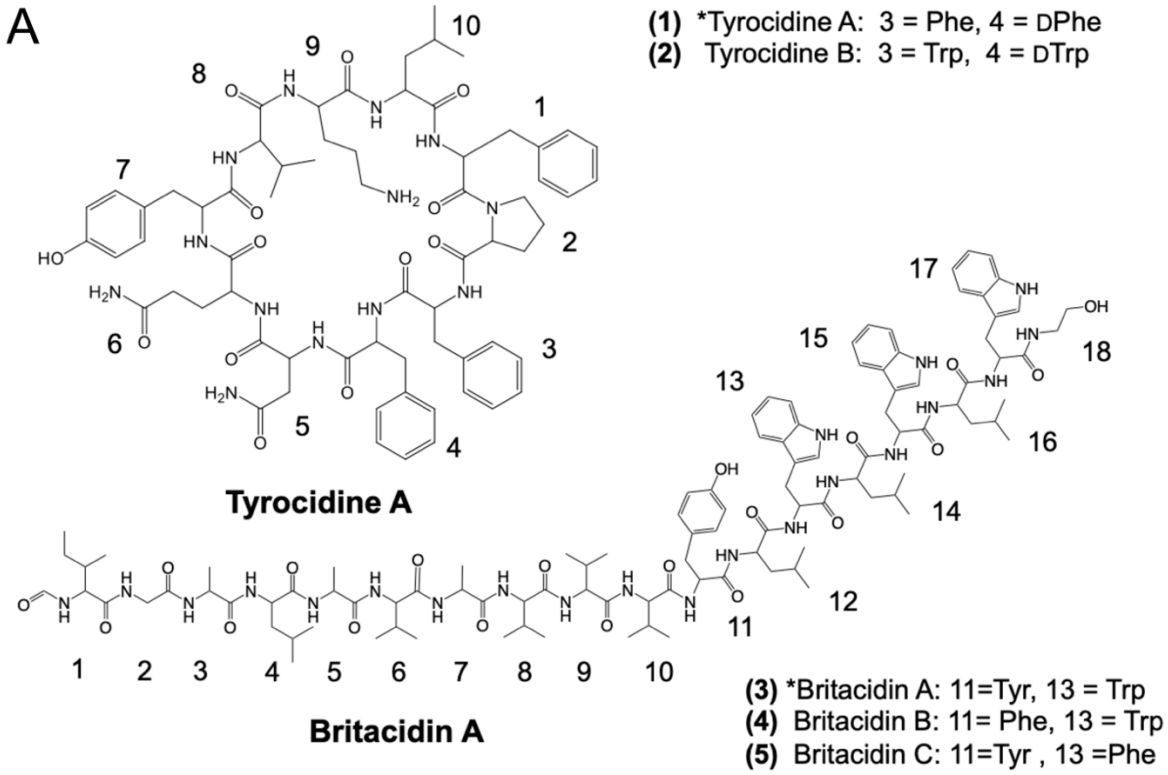
A
(1) *Tyrocidine A: 3 = Phe, 4 = DPhe
(2) Tyrocidine B: 3 = Trp, 4 = DTrp
Tyrocidine A
Britacidin A
(3) *Britacidin A: 11=Tyr, 13 = Trp
(4) Britacidin B: 11= Phe, 13 = Trp
(5) Britacidin C: 11=Tyr , 13 =Phe

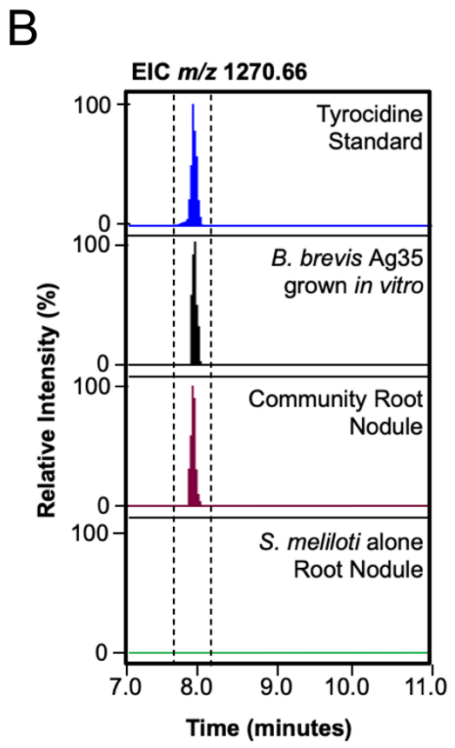
B
EIC m/z 1270.66
Tyrocidine Standard
B. brevis Ag35 grown in vitro
Community Root Nodule
S. meliloti alone Root Nodule
Relative Intensity (%)
Time (minutes)

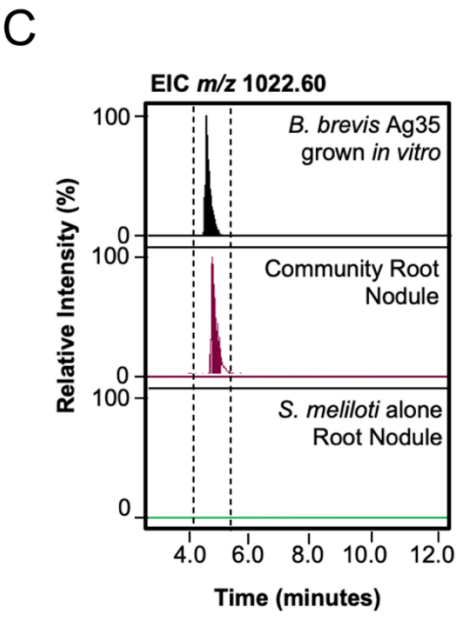
C
EIC m/z 1022.60
B. brevis Ag35 grown in vitro
Community Root Nodule
S. meliloti alone Root Nodule
Relative Intensity (%)
Time (minutes)

Figure 7: Britacidin and Gramicidin comparison at the chemical and genetic level. A) Chemical structure comparison of Britacidin A-C and Gramicidin A-D with blue boxes highlighting the structural differences. **B)** Comparison of the Gramicidin NRPS genes *lgrA-D* from *B. brevis* ATCC 8185 and the Britacidin NRPS genes *briA-D* from *B. brevis* Ag35. Amino acids incorporated by the AMP-binding domains (yellow) are listed within the gene described for *LgrA-D*. Stachelhaus alignments to *LgrA-D* were used for amino acid assignments for *briA-D*. **C)** Table highlighting the chemical positions 1, 7, 8, 11, and 13 (boxed in Fig. 7A) and their respective AMP-binding domain Stachelhaus codes, alignments, predictions and observed amino acids.

A

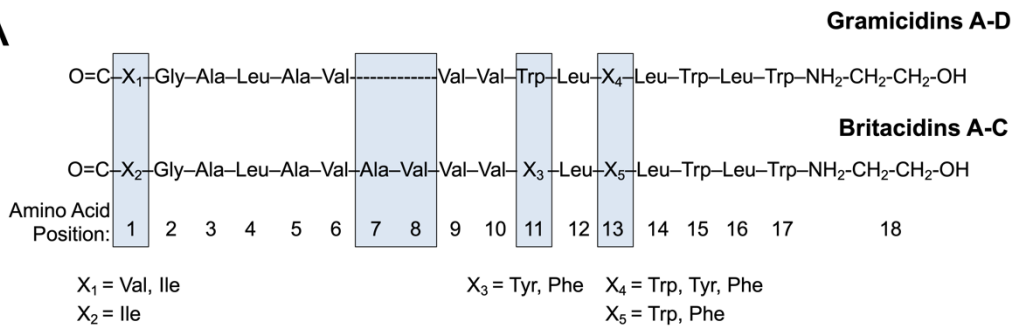

B

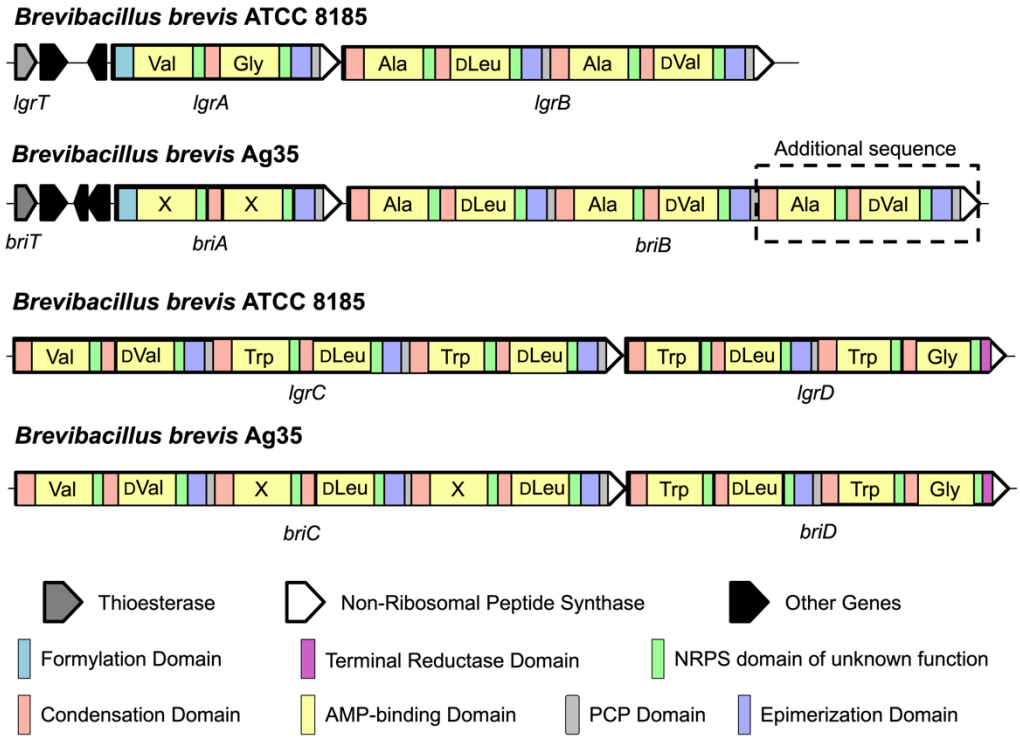

C

Position	*B. brevis* strain	Stachelhaus Code	Stachelhaus Prediction	Stachelhaus Confidence	Observed
1	ATCC 8185 Ag35	DglYiGGImK DgLfLGLIvK ** * *	Orn Gly	60% weak 70% weak	Val\Ile Ile
7	ATCC 8185 Ag35	---------- DLYNNALTYK **********	- Ala	- 100% strong	- Ala
8	ATCC 8185 Ag35	---------- DAfWLGGTFK **********	- Val	- 90% moderate	- Val
11	ATCC 8185 Ag35	DVSSIGcVcK DVAmVGcVcK ***	Trp Trp	80% moderate 70% weak	Trp Tyr,Phe
13	ATCC 8185 Ag35	DVSaIGcVtK DVsTIGcVtK *	Trp Arg	70% weak 70% weak	Trp,Tyr,Phe Trp,Phe

Chapter 3 Supplemental Tables

Table S4. Features unique to *Brevibacillus brevis* Ag35 after analysis presented in Figure 4C.

	Average RT (min)	**Average *m/z***	**Compound ID**
1	1.06	201.1717	-
2	1.35	215.1873	-
3	1.4	216.1909	-
4	5.81	617.3997	-
5	5.85	326.2809	-
6	5.85	348.2614	-
7	6.46	314.7053	-
8	7.84	1270.7094	-
9	7.84	1270.6665	Tyrocidine A $[M+H]^{+}$
10	7.85	635.8367	Tyrocidine A $[M+2H]^{2+}$
11	8.91	927.5285	-
12	9.89	1033.0829	Britacidin A $[M+Na+H]^{2+}$
13	10.7	453.3682	-

Table S5. Compounds verified in this study. Tyrocidines A and B produced by the bacterium, *B. brevis* Ag35, detected *in vitro* and *in planta,* were compared to an authentic standard and error was calculated. Britacidin A-C, produced by *B. brevis* Ag35, were detected either just *in vitro* (Britacidin B and C) or *in vitro* and *in planta* (Britacidin A). Heme B was detected *in planta* with LC-MS/MS and MALDI-IMS. Exact *in planta m/z* reported is from LC-MS/MS. Identification level (ID Level) assigned based on the identification standards set by Sumner LW, Amberg A, Barrett D, Beale MH, Beger R, Daykin CA, Fan TW, Fiehn O, Goodacre R, Griffin JL, Hankemeier T, Hardy N, Harnly J, Higashi R, Kopka J, Lane AN, Lindon JC, Marriott P, Nicholls AW, Reily MD, Thaden JJ, Viant MR. 2007. Metabolomics 3(3):211-221.

Compound ID			**Standard**		***in vitro***			***in planta***		
Common Name	Molecular Formula	Species	Expected *m/z*	Observed *m/z*	*m/z*	error (ppm)	ID Level	*m/z*	error (ppm)	ID Level
	C66H87N13O13	$[M+H]^+$	1270.6619	1270.6601	1270.6607*	0.5	1	1270.6649*	3.8	1
		$[M+Na]^+$	1292.6439	1292.6417	1292.6426	0.7		1292.6454	2.9	
Tyrocidine A		$[M+2H]^{2+}$	635.8346	635.8341	635.8338	0.5		635.8359	2.8	
	C68H88N14O13	$[M+H]^+$	1309.6728	1309.6726	1309.6730*	0.3	1			
Tyrocidine B		$[M+Na]^+$	1331.6547	1331.6552	1331.6656	7.8				
	C106H155N21O20	$[M+2H]^{2+}$	1022.0951	NA	1022.0960*	0.9	NA	1022.1071*	11.7	1#
		$[M+Na+H]^{2+}$	1033.0861	NA	1033.0848*	1.3	NA	1033.0948*	8.4	1#
		$[M+2Na]^{2+}$	1044.0771	NA	1044.0746*	2.4	NA	1044.0882*	10.6	1#
		$[M+H]^+$	2043.1830	NA	2043.1830*	0.0	NA	ND	ND	
Britacidin A		$[M+Na]^+$	2065.1649	NA	2065.1664*	0.7	NA	ND	ND	
	C106H155N21O19	$[M+2H]^{2+}$	1014.0977	NA	1014.1037*	5.9	NA			
		$[M+Na+H]^{2+}$	1025.0887	NA	1025.0944*	5.6	NA			
		$[M+2Na]^{2+}$	1036.0796	NA	1036.0848*	5.0	NA			
		$[M+H]^+$	2027.1881	NA	2027.1861*	1.0	NA			
Britacidin B		$[M+Na]^+$	2049.1700	NA	2049.1780	3.9	NA			
	C104H154N20O20	$[M+2H]^{2+}$	1002.5897	NA	1002.5936*	3.9	NA			
		$[M+Na+H]^{2+}$	1013.5807	NA	1013.5840*	3.3	NA			
		$[M+2Na]^{2+}$	1024.5716	NA	1024.5862*	14.2	NA			
		$[M+H]^+$	2004.1721	NA	2004.1725*	0.2	NA			
Britacidin C		$[M+Na]^+$	2026.1540	NA	2026.1586	2.3	NA			
Heme B	C34H32FeN4O4	$[M]^+$	616.1772					616.1750	3.6	1**

*MS2 acquired
ND = Not detected
**Identification based on protoporphyrin standard, MS2 provided in Figure S5
# Identification based on purified Britacidins mixture from *in vitro* conditions
NA = Not applicable, novel compound

Chapter 3 Supplemental Figures

Figure S4. Number of molecular features associated with the synthetic nodule community *in vitro* and *in planta*. Chemical extracts were prepared from three independent treatments of each microbe: alone on agar plates (*in vitro*), inoculated onto gnotobiotic alfalfa plants with *S. meliloti*, or inoculated onto gnotobiotic alfalfa plants with all other member of the synthetic nodule community. Chemical extracts were also prepared from a control in planta treatment of gnotobiotic alfalfa plants inoculated solely with *S. meliloti*. These chemical extracts were analyzed via untargeted LC/MS, resulting in feature lists for each treatment which are summarized here and in Figure 4. Number of features associated with;
(A) *S. melitoli,* **(B)** *Pantoea agglomerans* **(C)** *Pseudomonas sp*. **(D)** *Paenibacillus sp., and* **(E)** *B. brevis*.

A

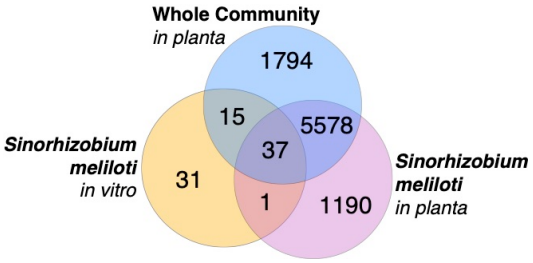
Whole Community
in planta
1794
15
5578
37
Sinorhizobium
meliloti
in vitro
31
1
1190
Sinorhizobium
meliloti
in planta

B

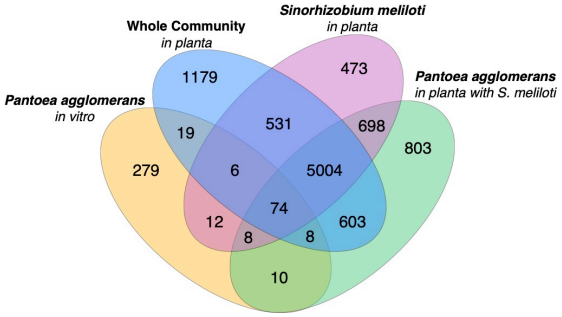
Whole Community
in planta
Sinorhizobium meliloti
in planta
Pantoea agglomerans
in vitro
Pantoea agglomerans
in planta with S. meliloti
1179
473
19
531
698
803
279
6
5004
12
74
603
8
8
10

C

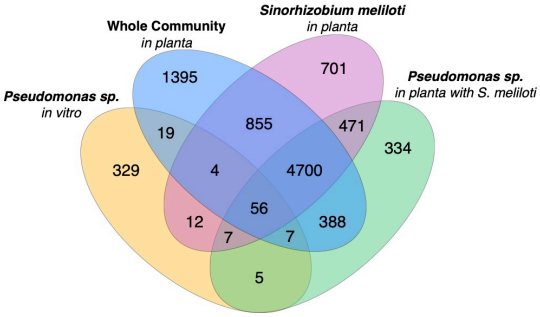
Whole Community
in planta
Sinorhizobium meliloti
in planta
Pseudomonas sp.
in vitro
Pseudomonas sp.
in planta with S. meliloti
1395
701
19
855
471
334
329
4
4700
56
12
7
7
388
5

D

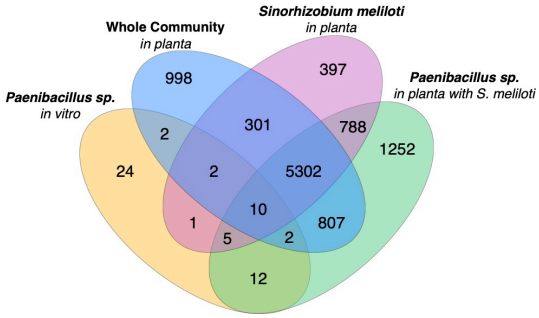
Whole Community
in planta
Sinorhizobium meliloti
in planta
Paenibacillus sp.
in vitro
Paenibacillus sp.
in planta with S. meliloti
998
397
2
301
788
1252
24
2
5302
10
1
807
5
2
12

E

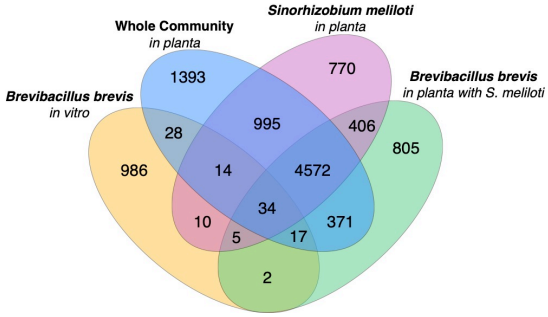
Whole Community
in planta
Sinorhizobium meliloti
in planta
Brevibacillus brevis
in vitro
Brevibacillus brevis
in planta with S. meliloti
1393
770
28
995
406
805
986
14
4572
34
10
5
17
371
2

Figure S5. Identification of Heme B *in planta*. MS2 fragmentation of *m/z* 616.2 found *in planta* compared to MS2 fragmentation of Protoporphyrin IX standard (Frontier Scientific). Chemical structure with breaks made in red dashed lines correspond with losses observed in the MS2 highlighted with red solid lines.

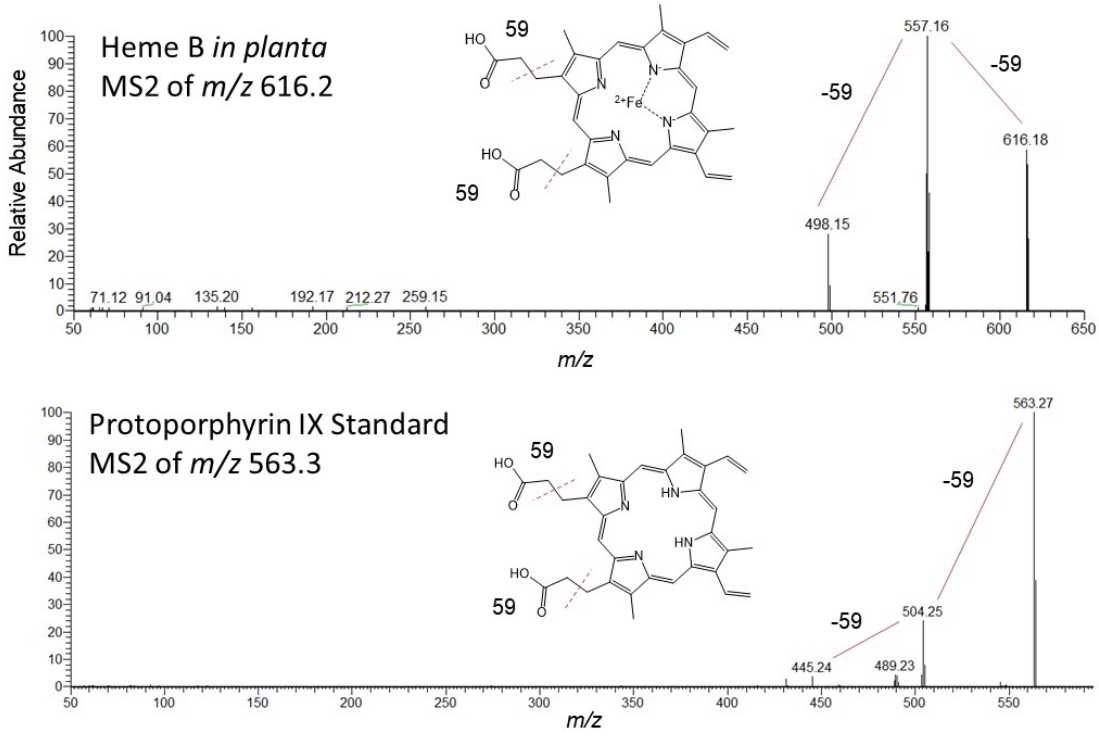

Figure S16: Ion maps for *m/z* 821.4 (A) and *m/z* 840.4 (B) from the same root nodule visualized in figure 5. Ions are unique to root nodule (non-matrix related) and demonstrate a uniform signal acquisition from the root nodule.

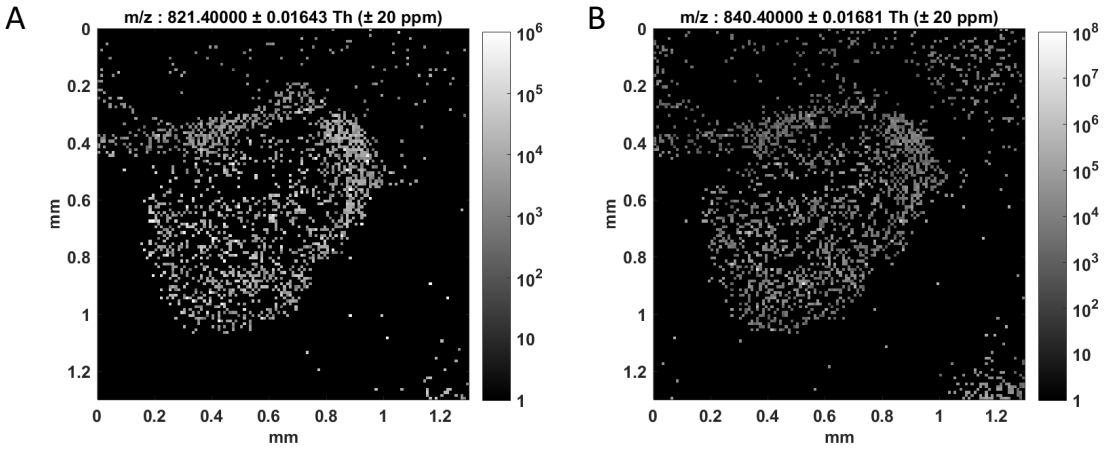

Figure S6. Identification of Tyrocidine A produced *in vitro* and *in planta*. Comparison of the MS2 of Tyrocidine A (*m/z* 1270.66) from a Tyrocidine authentic standard, methanol extracts from *Brevibacillus brevis* Ag35 (*in vitro)* and methanol extracts of the root nodule containing the community (*in planta)*.

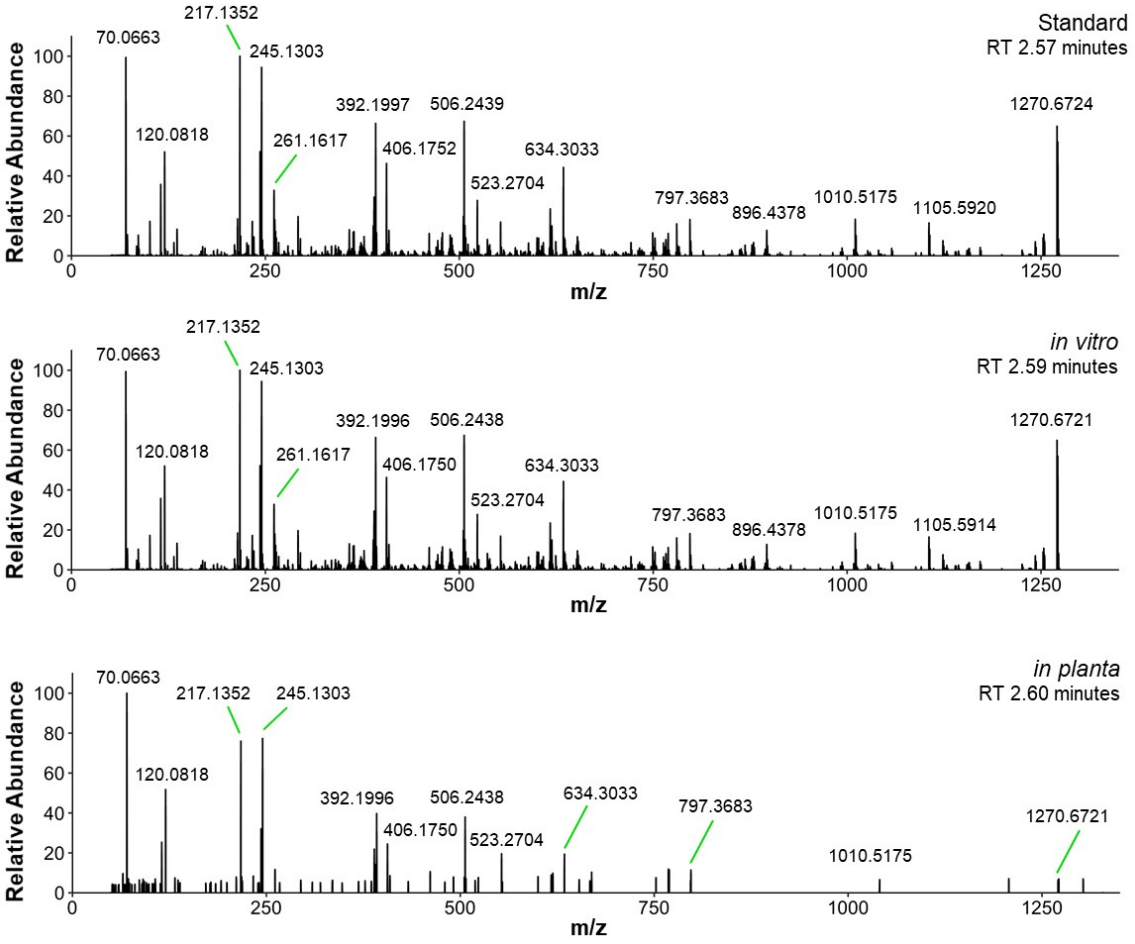

Figure S7. Identification of Tyrocidine B produced *in vitro*. Comparision of the MS2 of Tyrocidine B (*m/z 1309.67*), from a Tyrocidine authentic standard and methanol extracts from *Brevibacillus brevis* Ag35 (*in vitro)*.

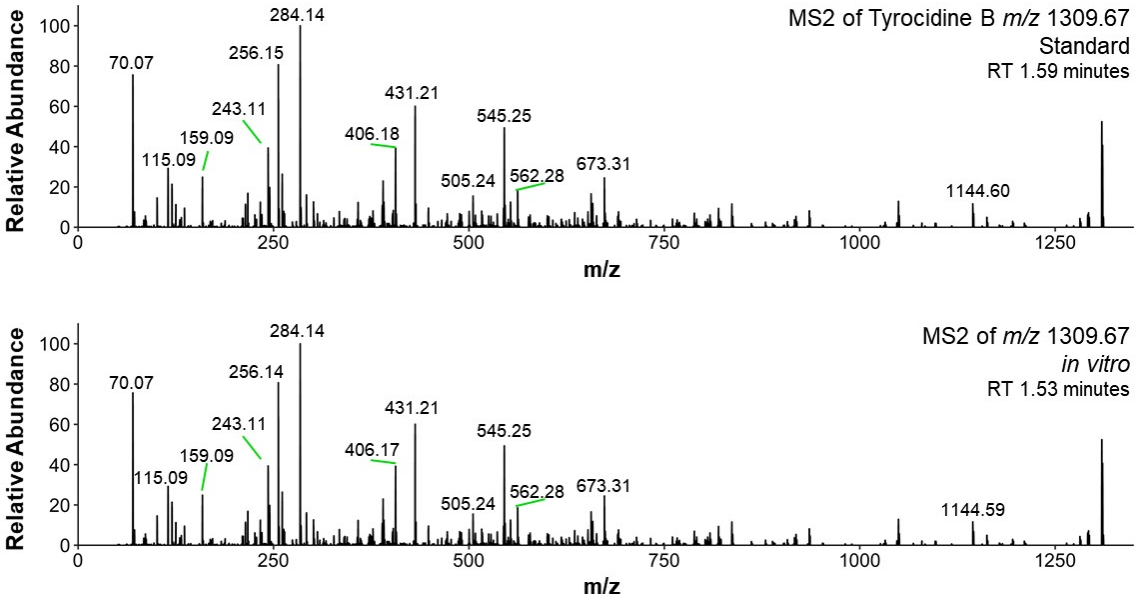

Figure S8. Britacidin A MS2 from three different charge states. Comparison of the MS2 of the $[M+2H]^{2+}$ of Britacidin A, *m/z* 1022.60 (dominant isotope of 1022.10), the $[M+H+Na]^{2+}$ of Britacidin A, , *m/z* 1033.60 (dominant isotope of 1033.08) and the $[M+2Na]^{2+}$ of Britacidin A, *m/z* 1044.59 (dominant isotope of 1044.07). The protonated species fragment similarly, however, the double sodiated species proves more difficult to fragment.

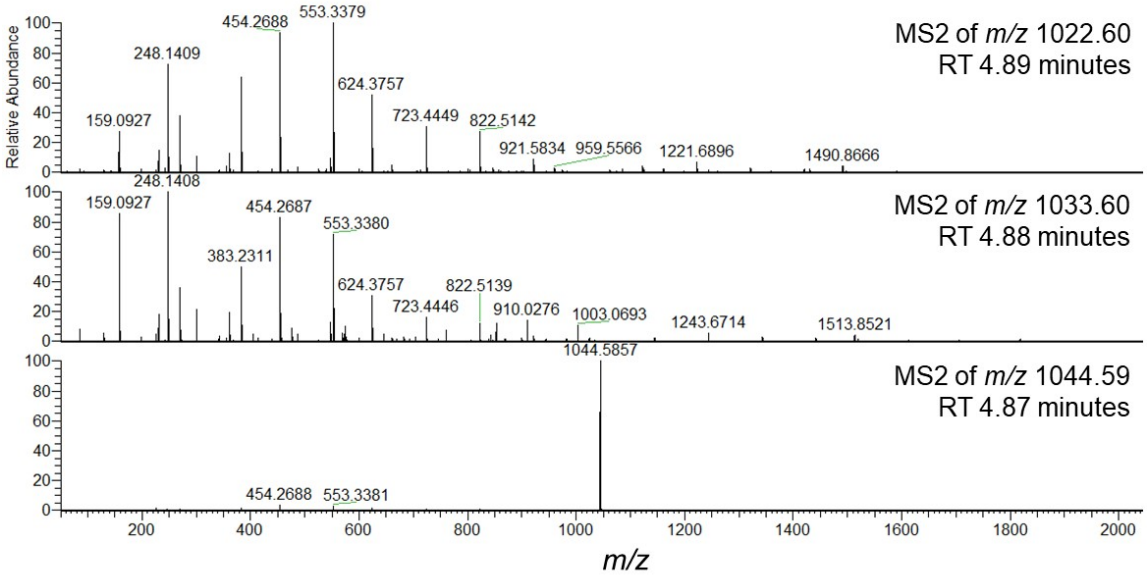

Figure S9. Gramicidin A and Britacidin A fragmentation. Comparison of the MS2 of the $[M+H]^+$ species of Gramicidin A from an authentic standard to the MS2 of the $[M+H]^+$ species of Britacidin A.

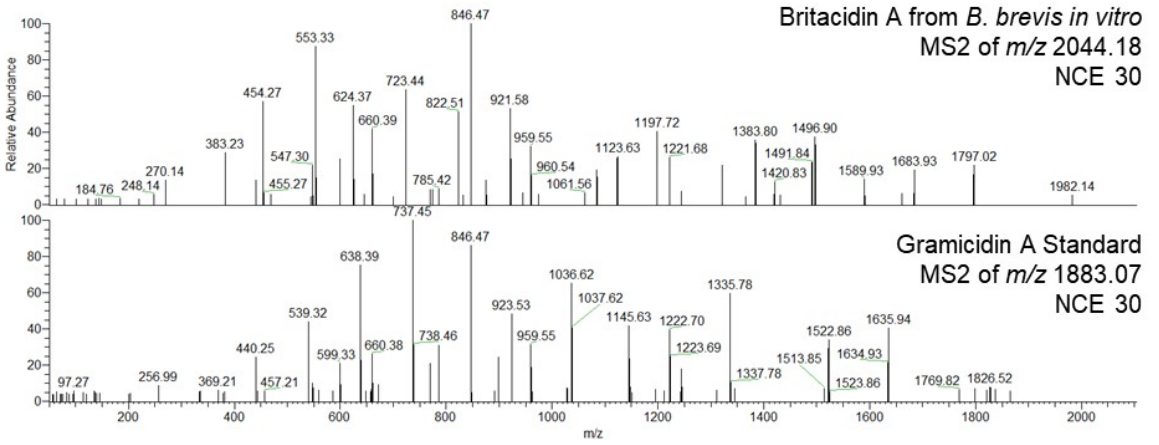

Figure S10. Britacidin A produced *in planta*. Comparison of the MS2 of the dominant ion species $[M+2H]^{2+}$, *m/z* 1022.60, identified *in vitro* and *in planta* at a NCE of 15.

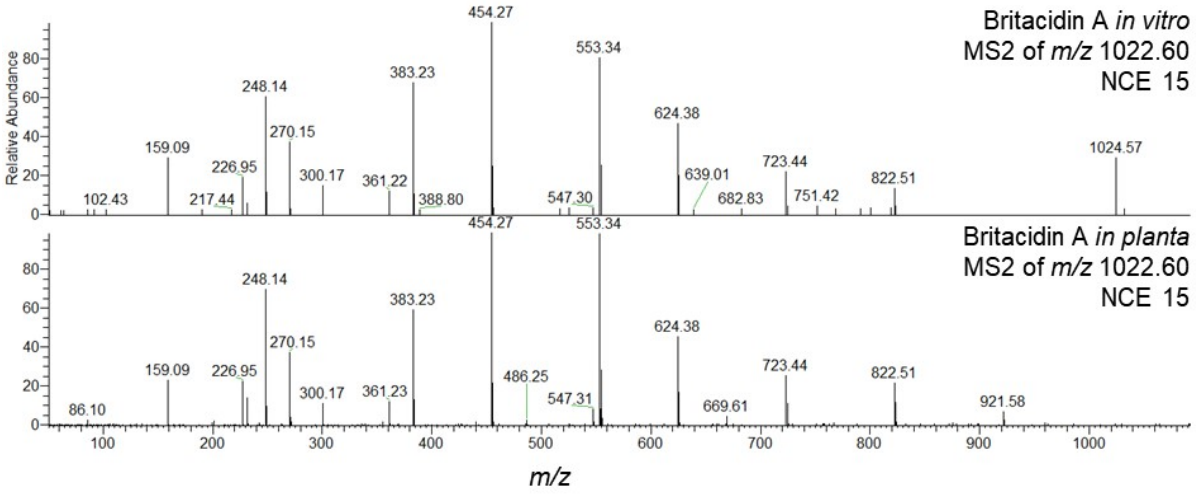

Figure S11. Fragmentation of Britacidin A. Britacidin A structure and table with corresponding y and b fragments identified through MS2 fragmentation of the $[M+H]^+$ and $[M+2H]^{2+}$ at a NCE of 15.

Britacidin A

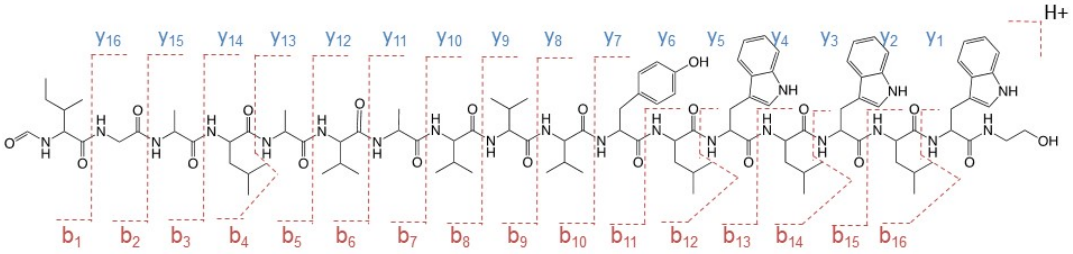

Britacidin A			**[M+H]+**		**[M+2H]2+**	
Fragment	**Chemical Formula**	**Theoretical *m/z***	**Observed *m/z***	**error (ppm)**	**Observed *m/z***	**error (ppm)**
y_1	[C13H18N3O2]+	248.1394	248.1387	2.8	248.1391	1.2
y_2	[C19H29N4O3]+	361.2234	361.224	1.7	361.2232	0.6
y_3	[C30H39N6O4]+	547.3027	547.3031	0.7	547.3027	0.0
y_4	[C36H50N7O5]+	660.3868	660.3875	1.1	660.3867	0.2
y_5	[C47H60N9O6]+	846.4661	846.4666	0.6	846.467	1.1
y_6	[C53H71N10O7]+	959.5502	959.5484	1.9	959.5511	0.9
y_7	[C62H80N11O9]+	1122.6135	1122.6156	1.9	1122.6143	0.7
y_8	[C67H89N12O10]+	1221.6819	1221.6809	0.8	1221.6832	1.1
y_9	[C72H98N13O11]+	1320.7503	1320.7539	2.7	1320.751	0.5
y_{10}	[C77H107N14O12]+	1419.8187	1419.8224	2.6	1419.8191	0.3
y_{11}	[C80H112N15O13]+	1490.8559	1490.8491	4.6	1490.8584	1.7
y_{12}	[C85H121N16O14]+	1589.9243	1589.9064	11.3	1589.9124	7.5
y_{13}	[C88H126N17O15]+	1660.9614	-	-	1660.9491	7.4
y_{14}	[C94H137N18O16]+	1774.0454	-	-	-	-
y_{15}	[C97H142N19O17]+	1845.0826	-	-	-	-
y_{16}	[C99H145N20O18]+	1902.104	-	-	-	-
b_1	[C7H12NO2]+	142.0863	-	-	142.0877	9.9
b_2	[C9H15N2O3]+	199.1077	-	-	199.1072	2.5
b_3	[C12H20N3O4]+	270.1448	270.1446	0.7	270.1445	1.1
b_4	[C18H31N4O5]+	383.2289	383.2289	0.0	383.2285	1.0

b_5	[C21H36N5O6]+	454.266	454.266	0.0	454.2656	0.9
b_6	[C26H45N6O7]+	553.3344	553.334	0.7	553.3341	0.5
b_7	[C29H50N7O8]+	624.3715	624.3721	1.0	624.3716	0.2
b_8	[C34H59N8O9]+	723.44	723.4413	1.8	723.4402	0.3
b_9	[C39H68N9O10]+	822.5084	822.5084	0.0	822.5086	0.2
b_{10}	[C44H77N10O11]+	921.5768	921.5776	0.9	921.5772	0.4
b_{11}	[C53H86N11O13]+	1084.6401	1084.6366	3.2	1084.635	4.7
b_{12}	[C59H97N12O14]+	1197.7242	1197.7273	2.6	1197.7216	2.2
b_{13}	[C70H107N14O15]+	1383.8035	1383.8077	3.0	1383.7985	3.6
b_{14}	[C76H118N15O16]+	1496.8875	1496.8839	2.4	1496.8804	4.7
b_{15}	[C87H128N17O17]+	1682.9669	1682.9652	1.0	1682.9528	8.4
b_{16}	[C93H139N18O18]+	1796.0609	-	-	-	-

Figure S12. Fragmentation of Britacidin B. Britacidin B structure and table with corresponding y and b fragments identified through MS2 fragmentation of the $[M+H]^+$ and $[M+2H]^{2+}$ at a NCE of 15.

Britacidin B

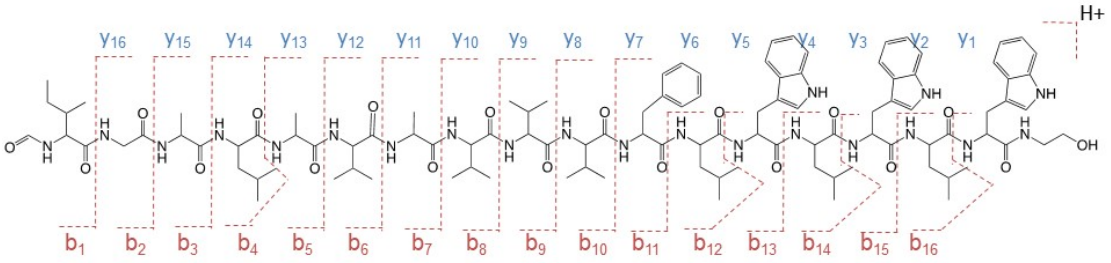

Britacidin B			**[M+H]+**		**[M+2H]2+**	
Fragment	**Chemical Formula**	**Theoretical *m/z***	**Observed *m/z***	**error (ppm)**	**Observed *m/z***	**error (ppm)**
y_1	[C13H18N3O2]+	248.1394	-	-	248.139	1.6
y_2	[C19H29N4O3]+	361.2234	-	-	361.2231	0.8
y_3	[C30H39N6O4]+	547.3027	547.3031	0.7	547.3026	0.2
y_4	[C36H50N7O5]+	660.3868	660.3827	6.2	660.3868	0.0
y_5	[C47H60N9O6]+	846.4661	846.463	3.7	846.4686	3.0
y_6	[C53H71N10O7]+	959.5502	959.5474	2.9	959.5506	0.4
y_7	[C62H80N11O8]+	1106.6186	1106.6095	8.2	-	-
y_8	[C67H89N12O9]+	1205.687	1205.6792	6.5	-	-
y_9	[C72H98N13O10]+	1304.7554	-	-	-	-
y_{10}	[C77H107N14O11]+	1403.8238	-	-	-	-
y_{11}	[C80H112N15O12]+	1474.8609	1474.852	6.0	-	-
y_{12}	[C85H121N16O13]+	1573.9294	-	-	-	-
y_{13}	[C88H126N17O14]+	1644.9665	-	-	-	-
y_{14}	[C94H137N18O15]+	1758.0505	-	-	-	-
y_{15}	[C97H142N19O16]+	1829.0876	-	-	-	-
y_{16}	[C99H145N20O17]+	1886.1091	-	-	-	-
b_1	[C7H12NO2]+	142.0863	-	-	142.088	12.0
b_2	[C9H15N2O3]+	199.1077	-	-	199.107	3.5
b_3	[C12H20N3O4]+	270.1448	-	-	270.1447	0.4
b_4	[C18H31N4O5]+	383.2289	383.2281	2.1	383.2286	0.8

b_5	[C21H36N5O6]+	454.266	454.2669	2.0	454.2655	1.1
b_6	[C26H45N6O7]+	553.3344	553.334	0.7	553.3333	2.0
b_7	[C29H50N7O8]+	624.3715	624.3693	3.5	624.3711	0.6
b_8	[C34H59N8O9]+	723.44	723.4376	3.3	723.441	1.4
b_9	[C39H68N9O10]+	822.5084	822.5043	5.0	822.5058	3.2
b_{10}	[C44H77N10O11]+	921.5768	921.5707	6.6	921.5748	2.2
b_{11}	[C53H86N11O12]+	1068.6452	1068.6441	1.0	-	-
b_{12}	[C59H97N12O13]+	1181.7293	1181.7196	8.2	-	-
b_{13}	[C70H107N14O14]+	1367.8086	1367.7955	9.6	-	-
b_{14}	[C76H118N15O15]+	1480.8926	1480.8791	9.1	-	-
b_{15}	[C87H128N17O16]+	1666.9719	1666.9419	18.0	-	-
b_{16}	[C93H139N18O17]+	1780.056	-	-	-	-

Figure S13. Fragmentation of Britacidin C. Britacidin C structure and table with corresponding y and b fragments identified through MS2 fragmentation of the $[M+H]^+$ and $[M+2H]^{2+}$ at a NCE of 15.

Britacidin C

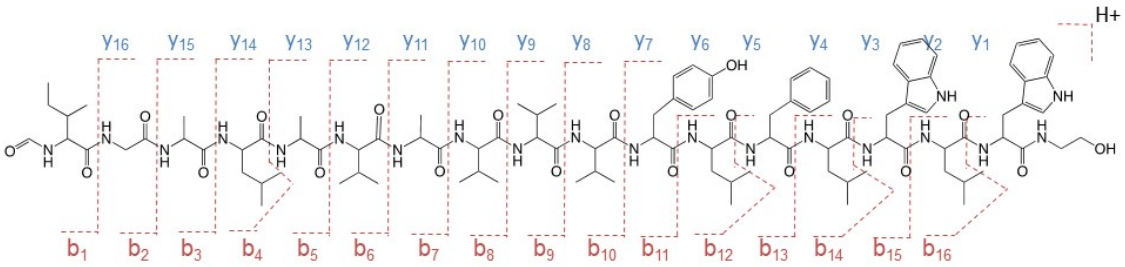

Britacidin C			**[M+H]+**		**[M+2H]2+**	
Fragment	**Chemical Formula**	**Theoretical *m/z***	**Observed *m/z***	**error (ppm)**	**Observed *m/z***	**error (ppm)**
y_1	[C13H18N3O2]+	248.1394	-	-	248.1391	1.2
y_2	[C19H29N4O3]+	361.2234	-	-	361.2233	0.3
y_3	[C30H39N6O4]+	547.3027	547.2997	5.5	547.303	0.5
y_4	[C36H50N7O5]+	660.3868	660.3856	1.8	660.3863	0.8
y_5	[C45H59N8O6]+	807.4552	807.4525	3.3	807.4564	1.5
y_6	[C51H70N9O7]+	920.5393	920.5344	5.3	920.5395	0.2
y_7	[C60H79N10O9]+	1083.6026	1083.5856	15.7	1083.607	3.7
y_8	[C65H88N11O10]+	1182.671	1182.6646	5.4	1182.672	0.7
y_9	[C70H97N12O11]+	1281.7394	1281.7368	2.0	1281.737	1.8
y_{10}	[C75H106N13O12]+	1380.8078	1380.8297	15.9	1380.809	0.9
y_{11}	[C78H111N14O13]+	1451.845	1451.8296	10.6	1451.849	3.0
y_{12}	[C83H120N15O14]+	1550.9134	-	-	1550.894	12.3
y_{13}	[C86H125N16O15]+	1621.9505	-	-	-	-
y_{14}	[C92H136N17O16]+	1735.0345	-	-	-	-
y_{15}	[C95H141N18O17]+	1806.0717	-	-	-	-
y_{16}	[C97H144N19O18]+	1863.0931	-	-	-	-
b_1	[C7H12NO2]+	142.0863	-	-	142.0879	11.3
b_2	[C9H15N2O3]+	199.1077	-	-	199.1075	1.0
b_3	[C12H20N3O4]+	270.1448	270.1451	1.1	270.1446	0.7

b_4	[C18H31N4O5]+	383.2289	383.2297	2.1	383.2286	0.8
b_5	[C21H36N5O6]+	454.266	454.2668	1.8	454.2657	0.7
b_6	[C26H45N6O7]+	553.3344	553.3334	1.8	553.334	0.7
b_7	[C29H50N7O8]+	624.3715	624.3724	1.4	624.3718	0.5
b_8	[C34H59N8O9]+	723.44	723.4406	0.8	723.4411	1.5
b_9	[C39H68N9O10]+	822.5084	822.5109	3.0	822.5092	1.0
b_{10}	[C44H77N10O11]+	921.5768	921.5604	17.8	921.5689	8.6
b_{11}	[C53H86N11O13]+	1084.6401	-	-	-	-
b_{12}	[C59H97N12O14]+	1197.7242	1197.7119	10.3	1197.713	9.0
b_{13}	[C68H106N13O15]+	1344.7926	1344.7817	8.1	1344.785	5.9
b_{14}	[C74H117N14O16]+	1457.8767	1457.8539	15.6	-	-
b_{15}	[C85H127N16O17]+	1643.956	-	-	-	-
b_{16}	[C91H138N17O18]+	1757.04	1757.0074	18.6	-	-

Figure S14. Comparison of the A domains from NRPS BriA-D and LgrA-D. Stachelhaus alignment of A domains from the NRPS of *Brevibacillus brevis* Ag35 (BriA-D) and *Brevibacillus brevis* ATCC 8185 (LgrA-D). Highlights in yellow are differences observed between amino acid sequences.

Stachelhaus alignment of all A Domains

BriA and LgrA	BriB and LgrB	BriC and LgrC	BriD and LgrD
Ag35 DgLfLGLIvK	Ag35 DVAnmAIiyK	Ag35 DAfWLGGTFK	Ag35 DVSSIGcVcK
ATCC DglYiGGImK	ATCC DVAnfAIiyK	ATCC DAfWLGGTFK	ATCC DVSSIGcVcK
Ag35 DAWFLGqVVK	Ag35 DAWFLGqVVK	Ag35 DAfWLGGTFK	Ag35 DAWFLGqVVK
ATCC DiaNlCIiYK	ATCC DAWFLGqVVK	ATCC DAfWLGGTFK	ATCC DAWFLGqVVK
	Ag35 DLYNNALTYK	Ag35 DVAmVGcVcK	Ag35 DVSSeGcVgK
	ATCC DLYNNALTYK	ATCC DVSSIGcVcK	ATCC DVSSeGcVgK
	Ag35 DAfWLGGTFK	Ag35 DAWFLGqVVK	Ag35 DLYNNcLvYK
	ATCC DAfWLGGTFK	ATCC DAWFLGqVVK	AtCC DLYNNcLvYK
	Ag35 DLYNNALTYK	Ag35 DVsTIGcVtK	
	ATCC ----------	ATCC DVSaIGcVtK	
	Ag35 DAfWLGGTFK	Ag35 DAWFLGqVVK	
	ATCC ----------	ATCC DAWFLGqVVK	

Chapter 4: Concluding Remarks

In this work, we demonstrate that the root nodule is an interesting system to study microbial interactions driven by antibiotics as defined in Chapter 1 and serves as a unique place for specialized metabolite discovery as demonstrated in Chapter 3. The root nodule is unique in that the binary interaction is sufficient for nodulation and nitrogen fixation. Therefore, this accessory community is not necessary for proper function of the rhizobia-legume symbiosis. However, as presented in Chapter 2, it appears that non-rhizobia are found cohabitating with rhizobia in this niche more often than not, suggesting the accessory community may be facultative in this niche. This occurrence of other members makes it an interesting system for studying microbial interactions.

Based on the work described in Chapter 2, it appears these microbes are interacting at some level of colonization of the root nodule. Current technical limitations make it difficult to study at which step these interactions are occurring, i.e., in the rhizosphere, the root, or within the root nodule. In addition, it is difficult to determine how colonization is happening for non-rhizobia, i.e., via the root hair, the root or through cracks in the root nodule tissue. Measuring recoverability of each member has shed some light as to what kind of interactions could be happening, i.e., cooperation or competition (Chapter 2). Further follow-up work with fluorescent bacteria could shed light onto how these microbes are entering the root nodule. Reporter strains could also shed light on when these microbes are interacting with one another.

The specialized metabolite potential was apparent when working with the final community members from this study as described in Chapter 2 and 3. *Brevibacillus brevis, Paenibacillus sp., Pseudomonas sp.* and *Pantoea agglomerans* all had the capacity to produce secondary metabolites with activity under *in vitro* conditions. This satisfied our model community requirements outlined in Chapter 1. The identities of most of these active metabolites remains unknown, however, detailed work on *B. brevis* led us to the discovery of a set of novel antimicrobial analogs we termed Britacidin A-C. Sequencing and annotation of the genome revealed the gene cluster. Follow-up work focusing on knocking out the gene cluster and measuring its impact on the recoverability of the community would help reveal the functional role of this molecule in the microbiome. However, more work needs to be done to understand the role this molecule might have on the physiology of *B. brevis* before any conclusions can be drawn.

In terms of drug discovery efforts, *B. brevis* was not the dominant member of the agricultural root nodules surveyed according to our sequencing data in Chapter 2. This suggests the plant selection approach taken in Chapter 2 led us to a discovery that may not have been possible under other conditions. It is unclear if we would have been able to isolate this microbe from bulk soil or from root tissue without the plant selection approach. This highlights the need for new approaches to isolate and identify microbes that could have interesting chemical potential.

Currently, this work highlights the importance of studying all parts of the microbiome. We learned in Chapter 2 that we cannot predict the interactions of a microbiome from the binary interactions alone. The interactome of a microbiome is complex and therefore, if possible, studying all possible combinations of a community could prove to highlight interactions that otherwise would not be detectable from binary networks. In Chapter 3, we learned that although a community has potential for antagonistic interactions, the spatial aspect of the microbiome can influence the persistence of otherwise susceptible members. The MALDI-IMS shed light on how *B. brevis* could be cohabitating with *S. meliloti*, despite making two antibiotics that inhibit its growth. Future work will need to focus on the impact of these antibiotics on the microbiome and on the overall nitrogen-fixing function of the root nodule

References

1. Fierer N. 2017. Embracing the unknown: Disentangling the complexities of the soil microbiome. Nat Rev Microbiol 15:579–590.
2. Sánchez-Cañizares C, Jorrín B, Poole PS, Tkacz A. 2017. Understanding the holobiont: the interdependence of plants and their microbiome. Curr Opin Microbiol 38:188–196.
3. Douglas AE. 2019. Simple animal models for microbiome research. Nat Rev Microbiol 17:764–775.
4. Thompson LR, Sanders JG, McDonald D, Amir A, Ladau J, Locey KJ, Prill RJ, Tripathi A, Gibbons SM, Ackermann G, Navas-Molina JA, Janssen S, Kopylova E, Vázquez-Baeza Y, González A, Morton JT, Mirarab S, Xu ZZ, Jiang L, Haroon MF, Kanbar J, Zhu Q, Song SJ, Kosciolek T, Bokulich NA, Lefler J, Brislawn CJ, Humphrey G, Owens SM, Hampton-Marcell J, Berg-Lyons D, McKenzie V, Fierer N, Fuhrman JA, Clauset A, Stevens RL, Shade A, Pollard KS, Goodwin KD, Jansson JK, Gilbert JA, Knight R, Agosto Rivera JL, Al-Moosawi L, Alverdy J, Amato KR, Andras J, Angenent LT, Antonopoulos DA, Apprill A, Armitage D, Ballantine K, Bárta J, Baum JK, Berry A, Bhatnagar A, Bhatnagar M, Biddle JF, Bittner L, Boldgiv B, Bottos E, Boyer DM, Braun J, Brazelton W, Brearley FQ, Campbell AH, Caporaso JG, Cardona C, Carroll JL, Cary SC, Casper BB, Charles TC, Chu H, Claar DC, Clark RG, Clayton JB, Clemente JC, Cochran A, Coleman ML, Collins G, Colwell RR, Contreras M, Crary BB, Creer S, Cristol DA, Crump BC, Cui D, Daly SE, Davalos L, Dawson RD, Defazio J, Delsuc F, Dionisi HM, Dominguez-Bello MG, Dowell R, Dubinsky EA, Dunn PO, Ercolini D, Espinoza RE, Ezenwa V, Fenner N, Findlay HS, Fleming ID, Fogliano V, Forsman A, Freeman C, Friedman ES, Galindo G, Garcia L, Garcia-Amado MA, Garshelis D, Gasser RB, Gerdts G, Gibson MK, Gifford I, Gill RT, Giray T, Gittel A, Golyshin P, Gong D, Grossart HP, Guyton K, Haig SJ, Hale V, Hall RS, Hallam SJ, Handley KM, Hasan NA, Haydon SR, Hickman JE, Hidalgo G, Hofmockel KS, Hooker J, Hulth S, Hultman J, Hyde E, Ibáñez-Álamo JD, Jastrow JD, Jex AR, Johnson LS, Johnston ER, Joseph S, Jurburg SD, Jurelevicius D, Karlsson A, Karlsson R, Kauppinen S, Kellogg CTE, Kennedy SJ, Kerkhof LJ, King GM, Kling GW, Koehler A V., Krezalek M, Kueneman J, Lamendella R, Landon EM, Lanede Graaf K, LaRoche J, Larsen P, Laverock B, Lax S, Lentino M, Levin II, Liancourt P, Liang W, Linz AM, Lipson DA, Liu Y, Lladser ME, Lozada M, Spirito CM, MacCormack WP, MacRae-Crerar A, Magris M, Martín-Platero AM, Martín-Vivaldi M, Martínez LM, Martínez-Bueno M, Marzinelli EM, Mason OU, Mayer GD, McDevitt-Irwin JM, McDonald JE, McGuire KL, McMahon KD, McMinds R, Medina M, Mendelson JR, Metcalf JL, Meyer F, Michelangeli F, Miller K, Mills DA, Minich J, Mocali S, Moitinho-Silva L, Moore A, Morgan-Kiss RM, Munroe P, Myrold D, Neufeld JD, Ni Y, Nicol GW, Nielsen S, Nissimov JI, Niu K, Nolan MJ, Noyce K, O'Brien SL, Okamoto N, Orlando L, Castellano YO, Osuolale O, Oswald W, Parnell J, Peralta-Sánchez JM, Petraitis P, Pfister C, Pilon-Smits E, Piombino P, Pointing SB, Pollock FJ, Potter C, Prithiviraj B, Quince C, Rani A, Ranjan R, Rao S, Rees AP, Richardson M, Riebesell U, Robinson C, Rockne KJ, Rodriguezl SM, Rohwer F, Roundstone W, Safran RJ, Sangwan N, Sanz V, Schrenk M, Schrenzel MD, Scott NM, Seger RL, Seguinorlando A, Seldin L, Seyler LM, Shakhsheer B, Sheets GM, Shen C, Shi Y, Shin H, Shogan BD, Shutler D, Siegel J, Simmons S, Sjöling S, Smith DP, Soler JJ, Sperling M, Steinberg PD, Stephens B, Stevens MA, Taghavi S, Tai V, Tait K, Tan CL, Taş N, Taylor DL, Thomas T, Timling I, Turner BL, Urich T, Ursell LK, Van Der Lelie D, Van Treuren W, Van

Zwieten L, Vargas-Robles D, Thurber RV, Vitaglione P, Walker DA, Walters WA, Wang S, Wang T, Weaver T, Webster NS, Wehrle B, Weisenhorn P, Weiss S, Werner JJ, West K, Whitehead A, Whitehead SR, Whittingham LA, Willerslev E, Williams AE, Wood SA, Woodhams DC, Yang Y, Zaneveld J, Zarraonaindia I, Zhang Q, Zhao H. 2017. A communal catalogue reveals Earth's multiscale microbial diversity. Nature 551:457–463.
5. Tyc O, van den Berg M, Gerards S, van Veen JA, Raaijmakers JM, de Boer W, Garbeva P. 2014. Impact of interspecific interactions on antimicrobial activity among soil bacteria. Front Microbiol 5:1–10.
6. Bertrand S, Bohni N, Schnee S, Schumpp O, Gindro K, Wolfender JL. 2014. Metabolite induction via microorganism co-culture: A potential way to enhance chemical diversity for drug discovery. Biotechnol Adv.
7. Traxler MF, Watrous JD, Alexandrov T, Dorrestein PC, Kolter R. 2013. Interspecies interactions stimulate diversification of the Streptomyces coelicolor secreted metabolome. MBio 4:1–12.
8. Wolfe BE, Dutton RJ. 2015. Fermented foods as experimentally tractable microbial ecosystems. Cell 161:49–55.
9. Takeshita T, Yasui M, Shibata Y, Furuta M, Saeki Y, Eshima N, Yamashita Y. 2015. Dental plaque development on a hydroxyapatite disk in young adults observed by using a barcoded pyrosequencing approach. Sci Rep 5:1–9.
10. Koch EJ, Miyashiro T, McFall-Ngai MJ, Ruby EG. 2014. Features governing symbiont persistence in the squid-vibrio association. Mol Ecol.
11. Sommer F, Bäckhed F. 2013. The gut microbiota-masters of host development and physiology. Nat Rev Microbiol.
12. Venturi V, Keel C. 2016. Signaling in the Rhizosphere. Trends Plant Sci.
13. Van Arnam E, Currie C, Clardy J. 2017. Defense contracts: molecular protection in insect-microbe symbioses. Chem Soc Rev.
14. Gulder TA, Moore BS. 2009. Chasing the treasures of the sea - bacterial marine natural products. Curr Opin Microbiol 12:252–260.
15. Mitri S, Richard Foster K. 2013. The Genotypic View of Social Interactions in Microbial Communities. Annu Rev Genet 47:247–273.
16. Zhang F, Berg M, Dierking K, Félix MA, Shapira M, Samuel BS, Schulenburg H. 2017. Caenorhabditis elegans as a model for microbiome research. Front Microbiol.
17. Elya C, Zhang V, Ludington WB, Eisen MB. 2016. Stable host gene expression in the gut of adult Drosophila melanogaster with different bacterial mono-associations. PLoS One.
18. Martinson VG, Danforth BN, Minckley RL, Rueppell O, Tingek S, Moran NA. 2011. A simple and distinctive microbiota associated with honey bees and bumble bees. Mol Ecol.
19. Niu B, Paulson JN, Zheng X, Kolter R. 2017. Simplified and representative bacterial community of maize roots. Proc Natl Acad Sci 114:e2450–e2459.
20. Doudna JA, Charpentier E. 2014. The new frontier of genome engineering with CRISPR-Cas9. Science (80-).
21. Hegge JW, Swarts DC, Van Der Oost J. 2018. Prokaryotic argonaute proteins: Novel genome-editing tools? Nat Rev Microbiol.
22. Wang M, Carver JJ, Phelan V V, Sanchez LM, Garg N, Peng Y, Nguyen DD, Watrous J, Kapono CA, Luzzatto-Knaan T, Porto C, Bouslimani A, Melnik A V, Meehan MJ, Liu W-T, Crüsemann M, Boudreau PD, Esquenazi E, Sandoval-Calderón M, Kersten RD, Pace LA, Quinn RA, Duncan KR, Hsu C-C, Floros DJ, Gavilan RG, Kleigrewe K, Northen T,

Dutton RJ, Parrot D, Carlson EE, Aigle B, Michelsen CF, Jelsbak L, Sohlenkamp C, Pevzner P, Edlund A, McLean J, Piel J, Murphy BT, Gerwick L, Liaw C-C, Yang Y-L, Humpf H-U, Maansson M, Keyzers RA, Sims AC, Johnson AR, Sidebottom AM, Sedio BE, Klitgaard A, Larson CB, Boya P CA, Torres-Mendoza D, Gonzalez DJ, Silva DB, Marques LM, Demarque DP, Pociute E, O'Neill EC, Briand E, Helfrich EJN, Granatosky EA, Glukhov E, Ryffel F, Houson H, Mohimani H, Kharbush JJ, Zeng Y, Vorholt JA, Kurita KL, Charusanti P, McPhail KL, Nielsen KF, Vuong L, Elfeki M, Traxler MF, Engene N, Koyama N, Vining OB, Baric R, Silva RR, Mascuch SJ, Tomasi S, Jenkins S, Macherla V, Hoffman T, Agarwal V, Williams PG, Dai J, Neupane R, Gurr J, Rodríguez AMC, Lamsa A, Zhang C, Dorrestein K, Duggan BM, Almaliti J, Allard P-M, Phapale P, Nothias L-F, Alexandrov T, Litaudon M, Wolfender J-L, Kyle JE, Metz TO, Peryea T, Nguyen D-T, VanLeer D, Shinn P, Jadhav A, Müller R, Waters KM, Shi W, Liu X, Zhang L, Knight R, Jensen PR, Palsson BØ, Pogliano K, Linington RG, Gutiérrez M, Lopes NP, Gerwick WH, Moore BS, Dorrestein PC, Bandeira N. 2016. Sharing and community curation of mass spectrometry data with Global Natural Products Social Molecular Networking. Nat Biotechnol 34:828–837.

23. Petras D, Jarmusch AK, Dorrestein PC. 2017. From single cells to our planet—recent advances in using mass spectrometry for spatially resolved metabolomics. Curr Opin Chem Biol 36:24–31.
24. Skinnider MA, Merwin NJ, Johnston CW, Magarvey NA. 2017. PRISM 3: Expanded prediction of natural product chemical structures from microbial genomes. Nucleic Acids Res.
25. Blin K, Medema MH, Kottmann R, Lee SY, Weber T. 2017. The antiSMASH database, a comprehensive database of microbial secondary metabolite biosynthetic gene clusters. Nucleic Acids Res.
26. Brown SP, Grillo MA, Podowski JC, Heath KD. 2020. Soil origin and plant genotype structure distinct microbiome compartments in the model legume Medicago truncatula. Microbiome 8:1–17.
27. Barker DG, Bianchi S, Blondon F, Dattée Y, Duc G, Essad S, Flament P, Gallusci P, Génier G, Guy P, Muel X, Tourneur J, Dénarié J, Huguet T. 1990. Medicago truncatula, a model plant for studying the molecular genetics of the Rhizobium-legume symbiosis. Plant Mol Biol Report 8:40–49.
28. Jones KM, Mendis HC, Queiroux C. 2013. Single-plant, Sterile Microcosms for Nodulation and Growth of the Legume Plant Medicago truncatula with the Rhizobial Symbiont Sinorhizobium meliloti. J Vis Exp e50916.
29. Xiao X, Chen W, Zong L, Yang J, Jiao S, Lin Y, Wang E, Wei G. 2017. Two cultivated legume plants reveal the enrichment process of the microbiome in the rhizocompartments. Mol Ecol 26:1641–1651.
30. Martínez-Hidalgo P. 2010. The nodule microbiome; N2-fixing rhizobia do not live alone. IEEE Electron Device Lett 0–24.
31. Davies J. 2013. Specialized microbial metabolites: Functions and origins. J Antibiot (Tokyo) 66:361–364.
32. Gaiero JR, McCall CA, Thompson KA, Day NJ, Best AS, Dunfield KE. 2013. Inside the root microbiome: bacterial root endophytes and plant growth promotion. Am J Bot 100:1738–1750.
33. Porras-Alfaro A, Bayman P. 2011. Hidden fungi, emergent properties: endophytes and

microbiomes. Annu Rev Phytopathol 49:291–315.
34. Bacon CW, White JF. 2016. Functions, mechanisms and regulation of endophytic and epiphytic microbial communities of plants. Symbiosis 68:87–98.
35. Whipps JM, Hand P, Pink D, Bending GD. 2008. Phyllosphere microbiology with special reference to diversity and plant genotype. J Appl Microbiol 105:1744–1755.
36. Andrews JH, Harris RF. 2000. The ecology and biogeography of microorganisms on plant surfaces. Annu Rev Phytopathol 38:145–180.
37. Compant S, Samad A, Faist H, Sessitsch A. 2019. A review on the plant microbiome: ecology, functions and emerging trends in microbial application. J Adv Res 19:29–37.
38. Berg G, Grube M, Schloter M, Smalla K. 2014. Unraveling the plant microbiome: looking back and future perspectives. Front Microbiol 5:1–7.
39. Herrera Paredes S, Gao T, Law TF, Finkel OM, Mucyn T, Teixeira PJPL, Salas González I, Feltcher ME, Powers MJ, Shank EA, Jones CD, Jojic V, Dangl JL, Castrillo G. 2018. Design of synthetic bacterial communities for predictable plant phenotypesPLoS Biology.
40. Naylor D, Coleman-Derr D. 2018. Drought stress and root-associated bacterial communities. Front Plant Sci 8:1–16.
41. Carlström CI, Field CM, Bortfeld-Miller M, Müller B, Sunagawa S, Vorholt JA. 2019. Synthetic microbiota reveal priority effects and keystone strains in the Arabidopsis phyllosphere. Nat Ecol Evol 3:1445–1454.
42. Shank EA. 2018. Considering the lives of microbes in microbial communities. mSystems 3:3–6.
43. Sasse J, Martinoia E, Northen T. 2018. Feed Your Friends: Do Plant Exudates Shape the Root Microbiome? Trends Plant Sci 23:25–41.
44. Helfrich EJN, Vogel CM, Ueoka R, Schäfer M, Ryffel F, Müller DB, Probst S, Kreuzer M, Piel J, Vorholt JA. 2018. Bipartite interactions, antibiotic production and biosynthetic potential of the Arabidopsis leaf microbiome. Nat Microbiol 3:909–919.
45. Lozano GL, Bravo JI, Garavito Diago MF, Park HB, Hurley A, Peterson SB, Stabb E V., Crawford JM, Broderick NA, Handelsman J. 2019. Introducing THOR, a model microbiome for genetic dissection of community behavior. MBio 10:1–14.
46. Raaijmakers JM, Mazzola M. 2012. Diversity and natural functions of antibiotics produced by beneficial and plant pathogenic bacteria. Annu Rev Phytopathol 50:403–424.
47. Brockwell J, Bottomley PJ, Thies JE. 1995. Manipulation of rhizobia microflora for improving legume productivity and soil fertility: A critical assessment. Plant Soil 174:143–180.
48. Brady NC, Weil RR. 2002. The nature and properties of soils, 13th Edition.
49. Long SR. 2001. Genes and signals in the rhizobium-legumes symbiosis. Plant Physiol 125:69–72.
50. Oldroyd GED, Murray JD, Poole PS, Downie JA. 2011. The rules of engagement in the legume-Rhizobial symbiosis. Annu Rev Genet 45:119–144.
51. Simms EL, Lee Taylor D. 2002. Partner choice in nitrogen-fixation mutualisms of legumes and rhizobia. Integr Comp Biol 42:369–380.
52. Porter SS, Simms EL. 2014. Selection for cheating across disparate environments in the legume-rhizobium mutualism. Ecol Lett 17:1121–1129.
53. Poole P, Ramachandran V, Terpolilli J. 2018. Rhizobia: From saprophytes to endosymbionts. Nat Rev Microbiol 16:291–303.
54. Desbrosses GJ, Stougaard J. 2011. Root nodulation: A paradigm for how plant-microbe

symbiosis influences host developmental pathways. Cell Host Microbe 10:348–358.
55. Young ND, Debellé F, Oldroyd GED, Geurts R, Cannon SB, Udvardi MK, Benedito VA, Mayer KFX, Gouzy J, Schoof H, Van De Peer Y, Proost S, Cook DR, Meyers BC, Spannagl M, Cheung F, De Mita S, Krishnakumar V, Gundlach H, Zhou S, Mudge J, Bharti AK, Murray JD, Naoumkina MA, Rosen B, Silverstein KAT, Tang H, Rombauts S, Zhao PX, Zhou P, Barbe V, Bardou P, Bechner M, Bellec A, Berger A, Bergès H, Bidwell S, Bisseling T, Choisne N, Couloux A, Denny R, Deshpande S, Dai X, Doyle JJ, Dudez AM, Farmer AD, Fouteau S, Franken C, Gibelin C, Gish J, Goldstein S, González AJ, Green PJ, Hallab A, Hartog M, Hua A, Humphray SJ, Jeong DH, Jing Y, Jöcker A, Kenton SM, Kim DJ, Klee K, Lai H, Lang C, Lin S, MacMil SL, Magdelenat G, Matthews L, McCorrison J, Monaghan EL, Mun JH, Najar FZ, Nicholson C, Noirot C, O'Bleness M, Paule CR, Poulain J, Prion F, Qin B, Qu C, Retzel EF, Riddle C, Sallet E, Samain S, Samson N, Sanders I, Saurat O, Scarpelli C, Schiex T, Segurens B, Severin AJ, Sherrier DJ, Shi R, Sims S, Singer SR, Sinharoy S, Sterck L, Viollet A, Wang BB, Wang K, Wang M, Wang X, Warfsmann J, Weissenbach J, White DD, White JD, Wiley GB, Wincker P, Xing Y, Yang L, Yao Z, Ying F, Zhai J, Zhou L, Zuber A, Dénarié J, Dixon RA, May GD, Schwartz DC, Rogers J, Quétier F, Town CD, Roe BA. 2011. The Medicago genome provides insight into the evolution of rhizobial symbioses. Nature 480:520–524.
56. Oke V, Long SR. 1999. Bacteroid formation in the Rhizobium-legume symbiosis. Curr Opin Microbiol 2:641–646.
57. Long SR. 1989. Rhizobium-legume nodulation: Life together in the underground. Cell 56:203–214.
58. Long SR, Staskawicz BJ. 1993. Prokaryotic plant parasites. Cell 73:921–935.
59. Lee A, Hirsch AM. 2006. Signals and responses: Choreographing the complex interaction between legumes and α- and β-rhizobia. Plant Signal Behav 1:161–168.
60. Hirsch AM, Larue TA, Doyle J. 1801. Is the legume nodule a modified root or stem or an organ suigeneris? CRC Crit Rev Plant Sci 16:361–392.
61. Gonzalez JE, Marketon MM. 2003. Quorum sensing in nitrogen-fixing rhizobia. Microbiol Mol Biol Rev 67:574–592.
62. Spaink HP. 1995. The molecular basis of infection and nodulation by rhizobia: The ins and outs of sympathogenesis. Annu Rev Phytopathol 33:345–368.
63. Schultze M, Kondorosi A. 1998. Regulation of symbiotic root nodule development. Annu Rev Genet 33–57.
64. Martínez-Hidalgo P, Hirsch AM. 2017. The nodule microbiome: N2-fixing rhizobia do not live alone. Phytobiomes J 1:70–82.
65. Xiao X, Chen W, Zong L, Yang J, Jiao S, Lin Y, Wang E, Wei G. 2017. Two cultivated legume plants reveal the enrichment process of the microbiome in the rhizocompartments. Mol Ecol 26:1641–1651.
66. Zgadzaj R, Garrido-Oter R, Jensen DB, Koprivova A, Schulze-Lefert P, Radutoiu S. 2016. Root nodule symbiosis in Lotus japonicus drives the establishment of distinctive rhizosphere, root, and nodule bacterial communities. PNAS 113:E7996–E8005.
67. Trujillo ME, Alonso-Vega P, Rodríguez R, Carro L, Cerda E, Alonso P, Martínez-Molina E. 2010. The genus Micromonospora is widespread in legume root nodules: The example of Lupinus angustifolius. ISME J 4:1265–1281.
68. Pini F, Frascella A, Santopolo L, Bazzicalupo M, Biondi EG, Scotti C, Mengoni A. 2012.

Exploring the plant-associated bacterial communities in Medicago sativa L. BMC Microbiol 12.
69. Travin DY, Watson ZL, Metelev M, Ward FR, Osterman IA, Khven IM, Khabibullina NF, Serebryakova M, Mergaert P, Polikanov YS, Cate JHD, Severinov K. 2019. Structure of ribosome-bound azole-modified peptide phazolicin rationalizes its species-specific mode of bacterial translation inhibition. Nat Commun 10.
70. Martínez-Hidalgo P, García JM, Pozo MJ. 2015. Induced systemic resistance against Botrytis cinerea by Micromonospora strains isolated from root nodules. Front Microbiol 6.
71. Senthilkumar M, Swarnalakshmi K, Govindasamy V, Lee YK, Annapurna K. 2009. Biocontrol potential of soybean bacterial endophytes against charcoal rot fungus, rhizoctonia bataticola. Curr Microbiol 58:288–293.
72. Lai WA, Asif A, Lin SY, Hung MH, Hsu YH, Liu YC, Shahina M, Shen FT, Young CC. 2015. Paenibacillus medicaginis sp. Nov. a chitinolytic endophyte isolated from a root nodule of alfalfa (medicago sativa l.). Int J Syst Evol Microbiol 65:3853–3860.
73. USDA. 2016. Alfalfa.
74. Van De Velde W, Guerra JCP, De Keyser A, De Rycke R, Rombauts S, Maunoury N, Mergaert P, Kondorosi E, Holsters M, Goormachtig S. 2006. Aging in legume symbiosis. A molecular view on nodule senescence in Medicago truncatula. Plant Physiol 141:711–720.
75. Sharaf H, Rodrigues RR, Moon J, Zhang B, Mills K, Williams MA. 2019. Unprecedented bacterial community richness in soybean nodules vary with cultivar and water status. Microbiome 7:1–18.
76. Leite J, Fischer D, Rouws LFM, Fernandes-Júnior PI, Hofmann A, Kublik S, Schloter M, Xavier GR, Radl V. 2017. Cowpea nodules harbor non-rhizobial bacterial communities that are shaped by soil type rather than plant genotype. Front Plant Sci 7:1–11.
77. Pessotti RC, Hansen BL, Traxler MF. 2018. In search of model ecological systems for understanding specialized metabolism. Msystems 3.
78. Cheng HP, Walker GC. 1998. Succinoglycan Is Required for Initiation and Elongation of Infection Threads during Nodulation of Alfalfa by Rhizobium meliloti. J Bacteriol 180:5183–5191.
79. Vincent JM. 1970. A Manual for the Practical Study of the Root-Nodule Bacteria.
80. Bor B, Bedree JK, Shi W, McLean JS, He X. 2019. Saccharibacteria (TM7) in the Human Oral Microbiome. J Dent Res 98:500–509.
81. Edwards JA, Santos-Medellín CM, Liechty ZS, Nguyen B, Lurie E, Eason S, Phillips G, Sundaresan V. 2018. Compositional shifts in root-associated bacterial and archaeal microbiota track the plant life cycle in field-grown rice. PLoS Biol 16:1–28.
82. Sturz A V, Christie BR, Matheson · B G, Nowak J, Matheson BG. 1997. Biodiversity of endophytic bacteria which colonize red clover nodules, roots, stems and foliage and their influence on host growth. Biol Fertil Soils 25:13–19.
83. Wigley K, Moot D, Wakelin SA, Laugraud A, Blond C, Seth K, Ridgway H. 2017. Diverse bacterial taxa inhabit root nodules of lucerne (Medicago sativa L.) in New Zealand pastoral soils. Plant Soil 420:253–262.
84. Ibáñez F, Angelini J, Taurian T, Tonelli ML, Fabra A. 2009. Endophytic occupation of peanut root nodules by opportunistic Gammaproteobacteria. Syst Appl Microbiol 32:49–55.
85. Simmons T, Caddell DF, Deng S, Coleman-Derr D. 2018. Exploring the root microbiome:

extracting bacterial community data from the soil, rhizosphere, and root endosphere. J Vis Exp.
86. Kozich JJ, Westcott SL, Baxter NT, Highlander SK, Schloss PD. 2013. Development of a dual-index sequencing strategy and curation pipeline for analyzing amplicon sequence data on the miseq illumina sequencing platform. Appl Environ Microbiol 79:5112–5120.
87. McMurdie PJ, Holmes S. 2013. Phyloseq: An R package for reproducible interactive analysis and graphics of microbiome census data. PLoS One 8.
88. Guo B, Wang Y, Sun X, Tang K. 2008. Bioactive natural products from endophytes: a review. Appl Biochem Microbiol 44:136–142.
89. Durán P, Thiergart T, Garrido-Oter R, Agler M, Kemen E, Schulze-Lefert P, Hacquard S. 2018. Microbial interkingdom interactions in roots promote Arabidopsis survival. Cell 175:973–983.
90. Okubara PA, Bonsall RF. 2008. Accumulation of Pseudomonas-derived 2,4-diacetylphloroglucinol on wheat seedling roots is influenced by host cultivar. Biol Control 46:322–331.
91. Raaijmakers JM, Bonsall RF, Weller DM. 1999. Effect of population density of Pseudomonas fluorescens on production of 2,4-diacetylphloroglucinol in the rhizosphere of wheat. Phytopathology 89:470–475.
92. Thomashow LS, Weller DM, Bonsall RF, Pierson LS. 1990. Production of the antibiotic phenazine-1-carboxylic acid by fluorescent Pseudomonas species in the rhizosphere of wheat. Appl Environ Microbiol 56:908–912.
93. Touré Y, Ongena M, Jacques P, Guiro A, Thonart P. 2004. Role of lipopeptides produced by Bacillus subtilis GA1 in the reduction of grey mould disease caused by Botrytis cinerea on apple. J Appl Microbiol 96:1151–1160.
94. Giddens SR, Houliston GJ, Mahanty HK. 2003. The influence of antibiotic production and pre-emptive colonization on the population dynamics of Pantoea agglomerans (Erwinia herbicola) Eh1087 and Erwinia amylovora in planta. Environ Microbiol 5:1016–1021.
95. Bonsall RF, Weller DM, Thomashow LS. 1997. Quantification of 2,4-diacetylphloroglucinol produced by fluorescent Pseudomonas spp. in vitro and in the rhizosphere of wheat. Appl Environ Microbiol 63:951–955.
96. Bergsma-Vlami M, Prins ME, Raaijmakers JM. 2005. Influence of plant species on population dynamics, genotypic diversity and antibiotic production in the rhizosphere by indigenous Pseudomonas spp. FEMS Microbiol Ecol 52:59–69.
97. Burkhead KD, Schisler DA, Slininger PJ. 1994. Pyrrolnitrin production by biological control agent Pseudomonas cepacia B37w in culture and in colonized wounds of potatoes. Appl Environ Microbiol 60:2031–2039.
98. Huang Z, Bonsall RF, Mavrodi D V., Weller DM, Thomashow LS. 2004. Transformation of Pseudomonas fluorescens with genes for biosynthesis of phenazine-1-carboxylic acid improves biocontrol of rhizoctonia root rot and in situ antibiotic production. FEMS Microbiol Ecol 49:243–251.
99. Kempf HJ, Bauer PH, Schroth MN. 1993. Herbicolin A associated with crown and roots of wheat after seed treatment with Erwinia herbicola B247 83:213–216.
100. Kinsella K, Schulthess CP, Morris TF, Stuart JD. 2009. Rapid quantification of Bacillus subtilis antibiotics in the rhizosphere. Soil Biol Biochem 41:374–379.
101. Maurhofer M, Keel C, Haas D, Defago G. 1995. Influence of plant species on disease suppression by Pseudomonas fluorescens strain CHAO with enhanced antibiotic

production. Plant Pathol 44:40–50.
102. Ligon JM, Hill DS, Hammer P, Torkewitz N, Hofmann D, Kempf H-J, van Pée K-H. 1999. Natural products with antimicrobial activity from Pseudomonas biocontrol bacteria. Pestic Chem Biosci 695:179–189.
103. Davison J. 1988. Plant Beneficial Bacteria. Nat Biotechnol 6:282–286.
104. Miklashevichs E, Röhrig H, Schell J, Schmidt J. 2001. Perception and signal transduction of Rhizobial NOD factors. CRC Crit Rev Plant Sci 20:373–394.
105. Debois D, Jourdan E, Smargiasso N, Thonart P, De Pauw E, Ongena M. 2014. Spatiotemporal monitoring of the antibiome secreted by bacillus biofilms on plant roots using MALDI mass spectrometry imaging. Anal Chem 86:4431–4438.
106. Pessotti RC, Hansen BL, Zacharia VM, Polyakov D, Traxler M. 2019. High spatial resolution imaging mass spectrometry reveals chemical heterogeneity across bacterial microcolonies. Anal Chem 91:14818–14823.
107. Nihorimbere V, Cawoy H, Seyer A, Brunelle A, Thonart P, Ongena M. 2012. Impact of rhizosphere factors on cyclic lipopeptide signature from the plant beneficial strain Bacillus amyloliquefaciens S499. FEMS Microbiol Ecol 79:176–191.
108. Meschke H, Walter S, Schrempf H. 2012. Characterization and localization of prodiginines from Streptomyces lividans suppressing Verticillium dahliae in the absence or presence of Arabidopsis thaliana. Environ Microbiol 14:940–952.
109. Abdelrahman M, El-Sayed MA, Hashem A, Abd-Allah EF, Alqarawi AA, Burritt DJ, Tran LSP. 2018. Metabolomics and transcriptomics in legumes under phosphate deficiency in relation to nitrogen fixation by root nodules. Front Plant Sci.
110. Veličković D, Agtuca BJ, Stopka SA, Vertes A, Koppenaal DW, Paša-Tolić L, Stacey G, Anderton CR. 2018. Observed metabolic asymmetry within soybean root nodules reflects unexpected complexity in rhizobacteria-legume metabolite exchange. ISME J 12:2335–2338.
111. Gemperline E, Li L. 2014. MALDI-mass spectrometric imaging for the investigation of metabolites in Medicago truncatula root Nodules. J Vis Exp.
112. Kessler N, Schuhmann H, Morneweg S, Linne U, Marahiel MA. 2004. The Linear Pentadecapeptide Gramicidin Is Assembled by Four Multimodular Nonribosomal Peptide Synthetases That Comprise 16 Modules with 56 Catalytic Domains. J Biol Chem 279:7413–7419.
113. Blin K, Shaw S, Steinke K, Villebro R, Ziemert N, Lee SY, Medema MH, Weber T. 2019. antiSMASH 5.0: updates to the secondary metabolite genome mining pipeline. Nucleic Acids Res 47:W81–W87.
114. Stachelhaus T, Mootz HD, Marahiel MA. 1999. The specificity-conferring code of adenylation domains in nonribosomal peptide synthetases. Chem Biol 6:493–505.
115. Nadell CD, Drescher K, Foster KR. 2016. Spatial structure, cooperation and competition in biofilms. Nat Rev Microbiol 14:589–600.
116. Reimer JM, Aloise MN, Harrison PM, Martin Schmeing T. 2016. Synthetic cycle of the initiation module of a formylating nonribosomal peptide synthetase. Nature 529:239–242.
117. Reimer JM, Eivaskhani M, Harb I, Guarné A, Weigt M, Martin Schmeing T. 2019. Structures of a dimodular nonribosomal peptide synthetase reveal conformational flexibility. Science (80-) 366:eaaw4388.
118. Dowle M, Srinivasan A. 2019. data.table: Extension of `data.frame`. R package version 1.12.6. https://CRAN.R-project.org/package=data.table.

119. Klinkert I, Chughtai K, Ellis SR, Heeren RMA. 2014. Methods for full resolution data exploration and visualization for large 2D and 3D mass spectrometry imaging datasets. Int J Mass Spectrom 362:40–47.
120. Bokhart MT, Nazari M, Garrard KP, Muddiman DC. 2018. MSiReader v1.0: Evolving Open-Source Mass Spectrometry Imaging Software for Targeted and Untargeted Analyses. J Am Soc Mass Spectrom 29:8–16.
121. Schneider CA, Rasband WS, Eliceiri KW. 2012. NIH Image to ImageJ: 25 years of Image Analysis. Nat Methods 9:671–675.